SAND2016-9958R

Results for the Aboveground Configuration of the Boiling Water Reactor Dry Cask Simulator

Fuel Cycle Research & Development

Prepared for
U.S. Department of Energy
Used Fuel Disposition Campaign

S. G. Durbin
E. R. Lindgren
Sandia National Laboratories

September 30, 2016

FCRD-UFD-2016-000433
SAND2016-xxxx

Sandia National Laboratories is a multi-mission laboratory managed and operated by Sandia Corporation, a wholly owned subsidiary of Lockheed Martin Corporation, for the U.S. Department of Energy's National Nuclear Security Administration under contract DE-AC04-94AL85000.

SUMMARY

The thermal performance of commercial nuclear spent fuel dry storage casks is evaluated through detailed numerical analysis. These modeling efforts are completed by the vendor to demonstrate performance and regulatory compliance. The calculations are then independently verified by the Nuclear Regulatory Commission (NRC). Carefully measured data sets generated from testing of full sized casks or smaller cask analogs are widely recognized as vital for validating these models. Recent advances in dry storage cask designs have significantly increased the maximum thermal load allowed in a cask in part by increasing the efficiency of internal conduction pathways and also by increasing the internal convection through greater canister helium pressure. These same canistered cask systems rely on ventilation between the canister and the overpack to convect heat away from the canister to the environment for both above and belowground configurations. While several testing programs have been previously conducted, these earlier validation attempts did not capture the effects of elevated helium pressures or accurately portray the external convection of aboveground and belowground canistered dry cask systems.

The purpose of the current investigation was to produce data sets that can be used to test the validity of the assumptions associated with the calculations used to determine steady-state cladding temperatures in modern dry casks that utilize elevated helium pressure in the sealed canister in an aboveground configuration.

An existing electrically heated but otherwise prototypic BWR Incoloy-clad test assembly was deployed inside of a representative storage basket and cylindrical pressure vessel that represents a vertical canister system. The symmetric single assembly geometry with well-controlled boundary conditions simplifies interpretation of results. The arrangement of ducting was used to mimic conditions for an aboveground storage configuration in a vertical, dry cask systems with canisters. Transverse and axial temperature profiles were measured for a wide range of decay power and helium cask pressures. Of particular interest was the evaluation of the effect of increased helium pressure on peak cladding temperatures (PCTs) for identical thermal loads.

All steady state peak temperatures and induced flow rates increased with increasing assembly power. Peak cladding temperatures decreased with increasing internal helium pressure for a given assembly power, indicating increased internal convection. In addition, the location of the PCT moved from near the top of the assembly to ~1/3 the height of the assembly for the highest (8 bar absolute) to the lowest (0 bar absolute) pressure studied, respectively. This shift in PCT location is consistent with the varying contribution of convective heat transfer proportional with of internal helium pressure.

TABLE OF CONTENTS

FIGURES

TABLES

ABBREVIATIONS/DEFINITIONS

ANSI	American National Standards Institute
BCS	BWR Cask Simulator
BWR	boiling water reactor
DAQ	data acquisition
DOE	Department of Energy
EPRI	Electric Power Research Institute
MSB	multi-assembly sealed basket
NRC	Nuclear Regulatory Commission
PID	proportional-integral-differential controller
PWR	pressurized water reactor
SCR	silicon controlled rectifier
SNF	spent nuclear fuel
SNL	Sandia National Laboratories
TC	thermocouple
VCC	ventilated concrete cask

RESULTS FOR THE ABOVEGROUND CONIFGURATION OF THE BOILING WATER REACTOR DRY REACTOR DRY CASK SIMULATOR

1 INTRODUCTION

The performance of commercial nuclear spent fuel dry storage casks is typically evaluated through detailed analytical modeling of the system's thermal performance. These modeling efforts are performed by the vendor to demonstrate the performance and regulatory compliance and are independently verified by the Nuclear Regulatory Commission (NRC). The majority of commercial dry storage casks in use today are aboveground. Both horizontally and vertically oriented aboveground dry cask systems are currently in use. Figure 1.1 shows a diagram for a typical vertical aboveground system. Cooling of the assemblies located inside the sealed canister is enhanced by the induced flow of air drawn in the bottom of the cask and exiting out the top of the cask.

Source: www.nrc.gov/reading-rm/doc-collections/fact-sheets/storage-spent-fuel-fs.html

Figure 1.1. Typical vertical aboveground storage cask system.

Figure 1.2 shows a diagram for a typical, vertical belowground system. For belowground configurations air is drawn in from the top periphery and channeled to the bottom where it then flows upward along the wall of the canister and exits out the top center of the cask.

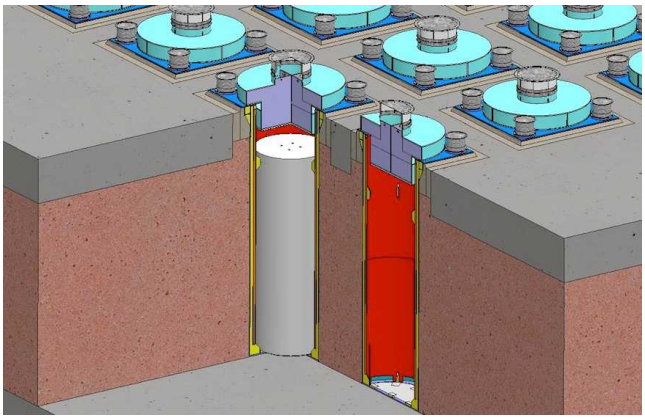

Source: www.holtecinternational.com/productsandservices/wasteandfuelmanagement/hi-storm/

Figure 1.2. Typical vertical belowground storage cask system.

Carefully measured data sets generated from testing of full sized casks or smaller cask analogs are widely recognized as vital for validating design and performance models. Numerous studies have been previously conducted [Bates, 1986; Dziadosz and Moore, 1986; Irino *et al.*, 1987; McKinnon *et al.*,1986]. Recent advances in dry storage cask designs have significantly increased the maximum thermal load allowed in a cask in part by increasing the efficiency of internal conduction pathways and by increasing the internal convection through greater canister helium pressure. These vertical, canistered cask systems rely on ventilation between the canister and the overpack to convect heat away from the canister to the environment for both above and belowground configurations. While several testing programs have been previously conducted, these earlier validation attempts did not capture the effects of elevated helium pressures or accurately portray the external convection of aboveground and belowground canistered dry cask systems. Previous cask performance validation testing did not capture these parameters. Thus the enhanced performance of modern dry storage casks cannot be fully validated using previous studies.

1.1 Objective

The purpose of this investigation is to produce a data set that can be used to test the validity of the assumptions associated with the calculations presently used to determine steady-state cladding temperatures in modern dry casks. These calculations are used to evaluate cladding integrity throughout storage cycle.

In addition, the results generated in this test series will supplement thermal data collected as part of the High Burnup Dry Storage Cask Project [EPRI, 2014]. It is anticipated that a shortened version of the thermal lance design deployed in the Cask Project will be installed in the BCS. The installation of this lance in the BCS assembly will allow the measurement of temperatures inside of a "guide tube" structure and directly on the fuel cladding.

1.2 Previous Studies

1.2.1 Small Scale, Single Assembly

Two single assembly investigations were documented in the mid-1980s [Bates, 1986; Irino *et al.*, 1987]. Both included electrically heated 15×15 pressurized water reactor (PWR) assemblies with thermocouples installed to directly measure the surface temperature of the cladding. In Bates (1986) the electrically heated assembly was instrumented with 57 TCs distributed over 7 axial

levels. In Irino *et al.* (1987) the electrically heated assembly was instrumented with 92 TCs distributed over 4 axial levels. In Bates (1986) a single irradiated 15×15 PWR assembly was also studied using 105 thermocouples distributed equally into each of the fifteen guide tubes at seven axial levels. All were limited to one atmosphere helium or air, and all imposed a constant temperature boundary condition on the outer cask wall in an attempt to achieve prototypic storage temperatures in the fuel assembly bundle.

1.2.2 Full Scale, Multi Assembly

A number of full scale multi-assembly cask studies were also documented in the mid-1980s to early 1990s, one for a BWR cask with unconsolidated fuel assemblies [McKinnon *et al*., 1986] and the others for PWR casks with both consolidated and unconsolidated fuel [Dziadosz *et al*., 1986; McKinnon *et al*., 1987; Creer *et al*., 1987; McKinnon *et al*.,1989; McKinnon *et al*., 1992]. Only in the most recent study was a ventilated cask design tested. In all studies the casks were studied with internal atmospheres ranging from vacuum up to 1.5 bar using air, nitrogen, or helium.

In the first study [McKinnon *et al*., 1986], 28 or 52 BWR assemblies with a total heat load of 9 or 15 kW respectively were contained in REA 2023 prototype steel-lead-steel cask with a water-glycol neutron shield. 38 TCs were installed on the cask interior. 24 of those were installed in direct contact with the center rod in 7 assemblies at up to 7 different elevations. 12 were installed on the basket at 3 different elevations. 2 TCs were installed in direct contact with a fuel rod located on the center outer face of an assembly. The cask was tested in a vertical and horizontal orientation with atmospheres of vacuum or nitrogen at 21 psia average or helium at 22 psia average.

In the earliest full scale PWR cask study [Dziadosz *et al*., 1986], twenty-one PWR assemblies with a total heat load of 28kW were contained in a Castor-V/21 cast iron/graphite cask with polyethylene rod neutron shielding. The interior of the cask was instrumented with sixty thermocouples deployed on ten lances located in eight guide tubes and two basket void spaces. Two of the assembly lances were installed into the center assembly. Note with the use of TC lances inside of the assembly guide tubes no direct fuel cladding temperatures were measured. The cask was tested in a vertical and horizontal orientation with atmospheres of vacuum or nitrogen at 0.57 bar or helium at 0.52 bar.

A relatively low total heat load of 12.6kW was tested in a Westinghouse MC-10 cask with 24 PWR assemblies [McKinnon *et al*., 1987]. The MC-10 has a forged steel body and distinctive vertical carbon steel heat transfer fins around the outer circumference. The outer surface of the cask was instrumented with 34 thermocouples. The interior of the cask was instrumented with 54 thermocouples deployed on 9 TC lances in 7 fuel assembly guide tubes and 2 basket void spaces. The cask was tested in a vertical and horizontal orientation and interior atmosphere was either a vacuum or 1.5 bar helium or air.

A pair of studies using the same TN-24 cask was tested with 24 PWR assemblies with 20.5 kW total output [Creer *et al*., 1987] or 24 consolidated fuel canisters with 23 kW total output [McKinnon *et al*.,1989]. The TN-24P has a forged steel body surrounded by a resin layer for neutron shielding. The resin layer is covered by a smooth steel outer shell. The TN-24P is a prototype version of the standard TN-24 cask with differences in the cask body thickness, basket material and neutron shield structure. The TN-24P also incorporates 14 thermocouples into the basket structure. In both studies the fuel was instrumented with 9 TC lances with 6 TCs per

lance, 7 in fuel guide tubes and 2 in simulated guide tubes in basket void spaces. The outside surface was instrumented with 35 TCs in the unconsolidated fuel study [Creer *et al*., 1987] and 27 TCs in the consolidated fuel study [McKinnon *et al*.,1989]. In both studies the cask was tested in a vertical and horizontal orientation with the interior atmosphere as either a vacuum or 1.5 bar helium or air. A seventh test was conducted in the consolidated fuel study [McKinnon *et al*.,1989] for a horizontal orientation under vacuum with insulated ends to simulate impact limiters.

None of the previous studies discussed so far included or accounted for internal ventilation of the cask. Both of the single assembly investigations imposed constant temperature boundary conditions [Bates, 1986; Irino *et al.*, 1987] and 4 full scale cask studies discussed so far [Dziadosz *et al*., 1986; McKinnon *et al*., 1987; Creer *et al*., 1987; McKinnon *et al*.,1989] considered externally cooled cask designs.

In only one previous study was a ventilated cask design considered, and this cask was the VSC-17 [McKinnon *et al*., 1992]. The VSC-17 cask system consists of a ventilated concrete cask (VCC) and a removable multi-assembly sealed basket (MSB). The VCC is steel lined and incorporates four inlet vents to the outside neat the bottom and four outlet vents near the top. When the MSB is placed inside the VCC an annular gap is formed and the vents allow air to be drawn in from the bottom through the annular gap and out the top vents. The lid on the MSB is a specially designed bolted closure that seals the basket interior and closes off the top of the cask above the top vents. The VSC-17 is a specially designed test version (holding 17 PWR assemblies) of the commercial VSC-24 cask (holding 24 PWR assemblies). The VSC-17 is smaller and lighter and incorporates the bolted lid to facilitate testing. The VSC-24 is larger and utilizes a welded lid canister for containing the spent fuel assemblies.

In the investigation of the VSC-17 cask, 17 consolidated PWR fuel canisters with a total heat load of 14.9 kW were utilized. The cask system was instrumented with 98 thermocouples. Forty-two of these were deployed on 7 TC lances with 6 TCs each. Six lances were installed in the fuel canisters and one was installed in a basket void space. Nine TCs were located on the outer MSB wall and 9 TCs were located on the inner VCC liner. Ten TCs were embedded in the VCC concrete wall. One TC was located at each vent inlet and outlet. Thirteen TCs were located on the outer cask surface and weather cover. Testing consisted of six runs all in a vertical orientation. In 4 tests the MSB was filled with helium at an average pressure of 0.95 bar. The vents were either all unblocked, or the inlets were half blocked, or the inlets were fully blocked or both the inlets and outlets were fully blocked. The other two runs were with unblocked vents and 0.84 bar nitrogen or vacuum.

1.2.3 Uniqueness of Present Test Series

The present investigation differs in a number of significant ways. Principle among these is that the canister pressure vessel was tested with helium pressures up to 8 bar and assembly powers up to 5000 W until a steady state temperature profile was established. During the apparatus heating, the helium pressure was controlled to be constant to within ±0.05 psi. Additionally, ventilated design boundary conditions for aboveground configuration was explicitly simulated. The experimental approach of the present study is different than the previous studies. Rather than striving to achieve prototypic peak clad temperatures by artificially imposing a temperature boundary condition on the canister wall, the present study represents the physics of near-prototypic boundary conditions.

2 APPARATUS AND PROCEDURES

2.1 General Construction

The general design details are shown in Figure 2.1. An existing electrically heated but otherwise prototypic BWR Incoloy-clad test assembly was deployed inside of a representative storage basket and cylindrical pressure vessel that represents the canister. The symmetric single assembly geometry with well-controlled boundary conditions simplifies interpretation of results. Various configurations of outer concentric ducting were used to mimic conditions for aboveground storage configurations of vertical, dry cask systems with canisters. Radial and axial temperature profiles were measured for a wide range of decay power and canister helium pressures. Of particular interest was the evaluation of the effect of increased helium pressure on heat load for the aboveground configuration. The External mass flow rates and convective heat transfer coefficients are calculated from measurements of the external cooling flows.

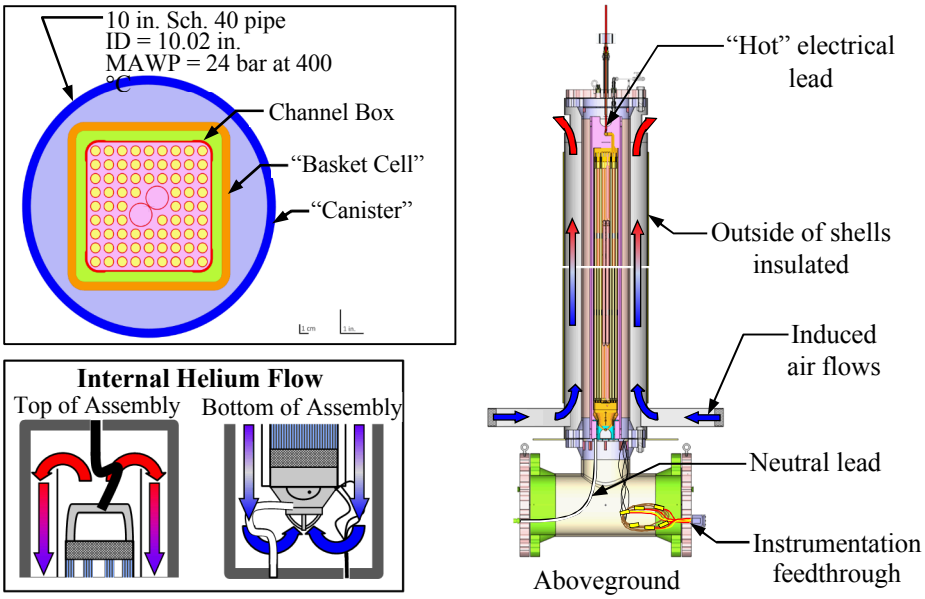

Figure 2.1. General design details sowing the plan view (upper left), the internal helium flow (lower left) and the external air flow for the above ground (right).

Figure 2.2 shows some of the carbon steel components used to fabricate the pressure vessel. The 4.572 m (180 in.) long vertical test section is made from 0.254 m (10 in.) Schedule 40 pipe welded to Class 300 flanges. The 0.356 × 0.254 m (14 × 10 in.) Schedule 40 reducing tee is needed to facilitate routing over 150 thermocouples (TCs) out of the pressure vessel. Blind flanges with threaded access ports for TC and power lead pass-throughs are bolted to the top of the vertical test stand section and the sides of the reducing tee. The maximum allowable working pressure is 24 bar at 400 °C. Bar stock tabs were welded inside the 0.254 m (10 in.) flange on the tee to support the test assembly and allow an insulated top boundary condition.

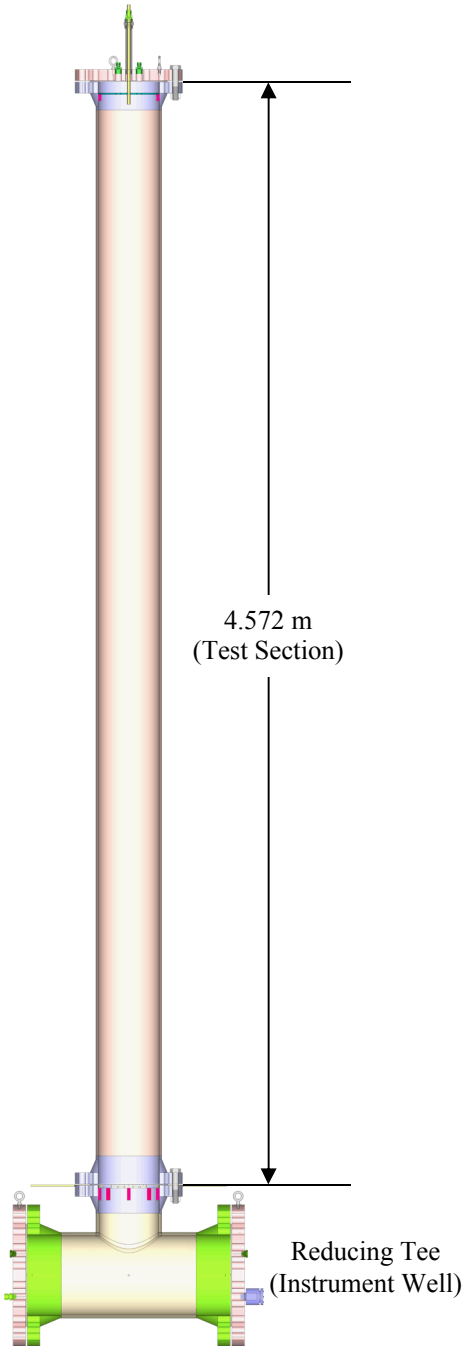

Figure 2.2. Carbon steel pressure vessel.

The test configurations will be assembled and operated inside of the Cylindrical Boiling (CYBL) test facility, which is the same facility used for earlier fuel assembly studies [Lindgren and Durbin, 2007]. CYBL is a large stainless steel containment vessel repurposed from earlier flooded containment/core retention studies sponsored by DOE. Since then CYBL has served as an excellent general-use engineered barrier for the isolation of high-energy tests. The outer vessel is 5.1 m in diameter and 8.4 m tall (16.7 ft. in diameter and 27.6 feet tall) and constructed with 9.5 mm (0.375 in.) thick stainless steel walls. Figure 2.3 shows an idealized representation of the CYBL facility with the aboveground version of the test BCS inside.

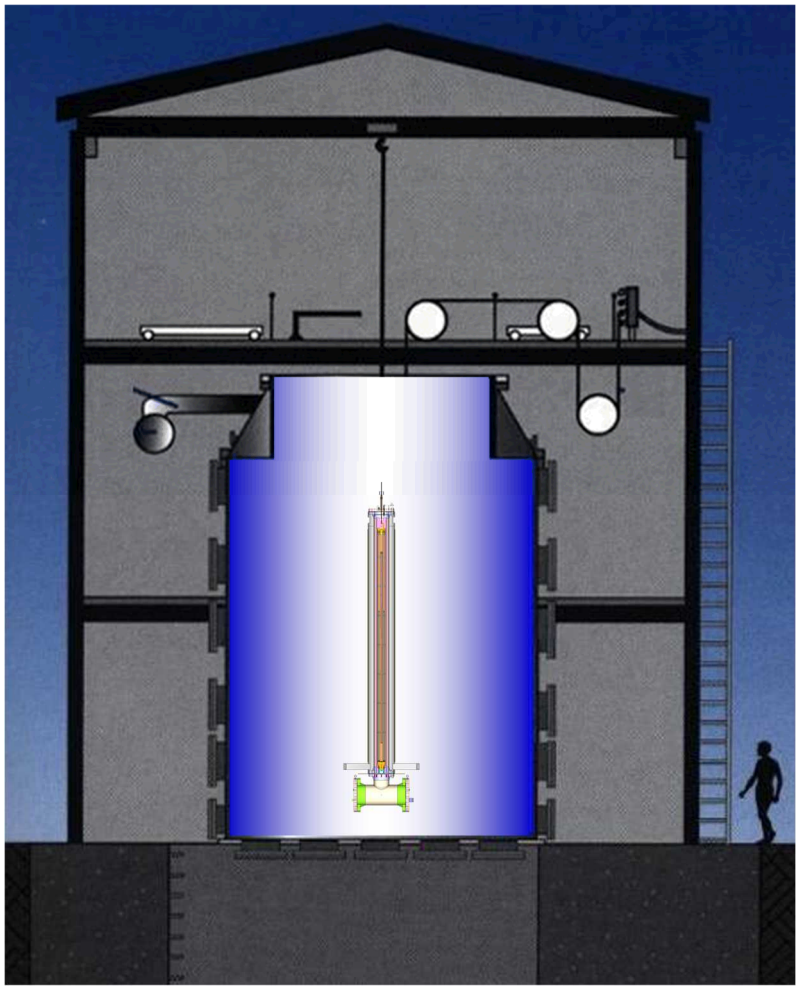

Figure 2.3 CYBL facility housing the aboveground version of the BWR cask simulator.

2.2 Design of the Heated Fuel Bundle

The highly prototypic fuel assembly was modeled after a 9×9 BWR. Commercial components were purchased to create the assembly including the top and bottom tie plates, spacers, water rods, channel box, and all related assembly hardware (see Figure 2.4). Incoloy heater rods were substituted for the fuel rod pins for heated testing. Due to fabrication constraints the diameter of the Incoloy heaters was slightly smaller than prototypic pins, 10.9 mm versus 11.2 mm. The slightly simplified Incoloy mock fuel pins were fabricated based on drawings and physical examples from the nuclear component supplier. The dimensions of the assembly components are listed below in Table 2.1.

Table 2.1. Dimensions of assembly components in the 9×9 BWR

Description	Lower (Full) Section	Upper (Partial) Section
Number of pins	74	66
Pin diameter (mm)	10.9	10.9
Pin pitch (mm)	14.4	14.4
Pin separation (mm)	3.48	3.48
Water rod OD (main section) (mm)	24.9	24.9
Water rod ID (mm)	23.4	23.4
Nominal channel box ID (mm)	134	134
Nominal channel box OD (mm)	139	139

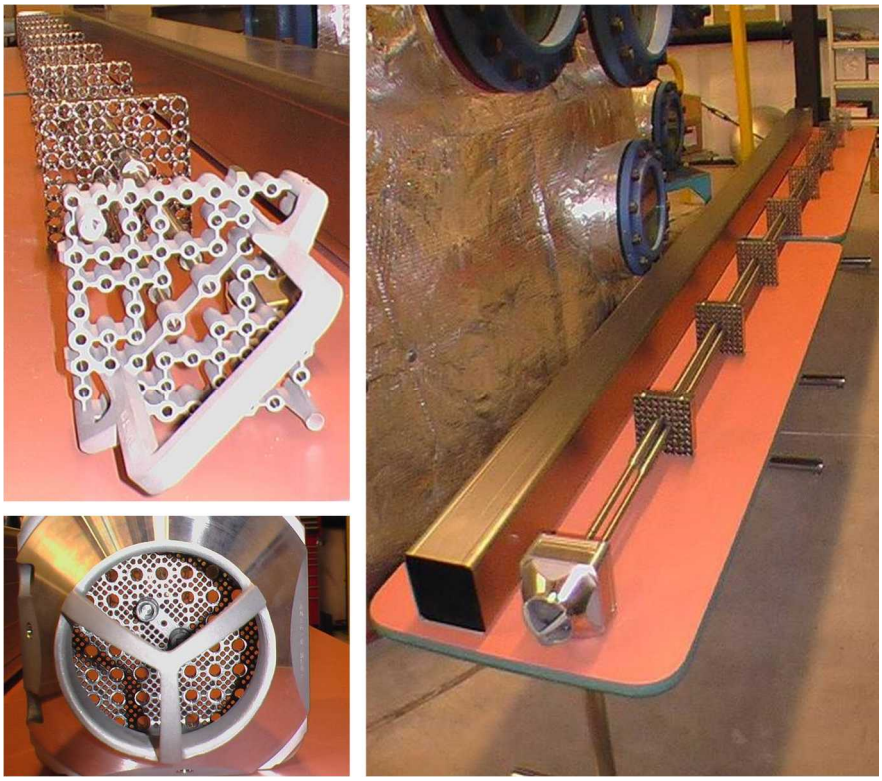

Figure 2.4. Typical 9×9 BWR components used to construct the test assembly including top tie plate (upper left), bottom tie plate (bottom left) and channel box and spacers assembled onto the water rods (right).

The thermocouples used are ungrounded junction Type K with an Incoloy sheath diameter of 0.762 mm (0.030 in.) held in intimate contact with the cladding by a thin Nichrome shim. This shim is spot welded to the cladding as shown in Figure 2.5. The TC attachment method allows the direct measurement of the cladding temperature.

Figure 2.5. Typical TC attachment to heater rod.

2.3 Instrumentation

The test apparatus was instrumented with thermocouples (TCs) for temperature measurements, pressure transducers to monitor the internal helium pressure, and hot wire anemometers for flow velocity measurement in the exterior ducting. Volumetric flow controllers were used to calibrate the hotwire probes. Voltage, amperage, and electrical power transducers were used for monitoring the electrical energy input to the test assembly.

Ninety-seven thermocouples were previously installed on the BWR test assembly. Details of the BWR test assembly and TC locations are described elsewhere [Lindgren and Durbin, 2007]. Additional thermocouples were installed on the other major components of the test apparatus such as the channel box, storage basket, canister wall, and exterior air ducting. TC placement on these components is designed to correspond with the existing TC placement in the BWR assembly.

Hot wire anemometers were chosen to measure the inlet flow rate because this type of instrument is sensitive and robust while introducing almost no unrecoverable flow losses. Due to the nature of the hot wire measurements, best results are achieved when the probe is placed in an isothermal, unheated gas flow. Calibration of the hot wires was performed by imposing a known mass flow rate of air through the ducting with the hot wires in place.

2.3.1 Thermocouples (TCs)

2.3.1.1 BWR Assembly TC locations

The existing electrically heated prototypic BWR Incoloy-clad test assembly was previously instrumented with thermocouples in a layout shown in Figure 2.6. The assembly TCs are arranged in axial and radial arrays. The axial cross-section is depicted in Figure 2.6a and radial cross-sections are shown in Figure 2.6b. The axial array A1 has TCs nominally spaced every 0.152 m (6 in.) starting from the top of the bottom tie plate (z_o = 0 reference plane). Axial array A2 has TCs nominally spaced every 0.305 m (12 in.) and the radial arrays are nominally spaced every 0.610 m (24 in.). The spacings are referred to as nominal due to a deviation at the 3.023 m

(119 in.) elevation because of interference by a spacer. Note that the TCs in the axial array intersect with the radial arrays.

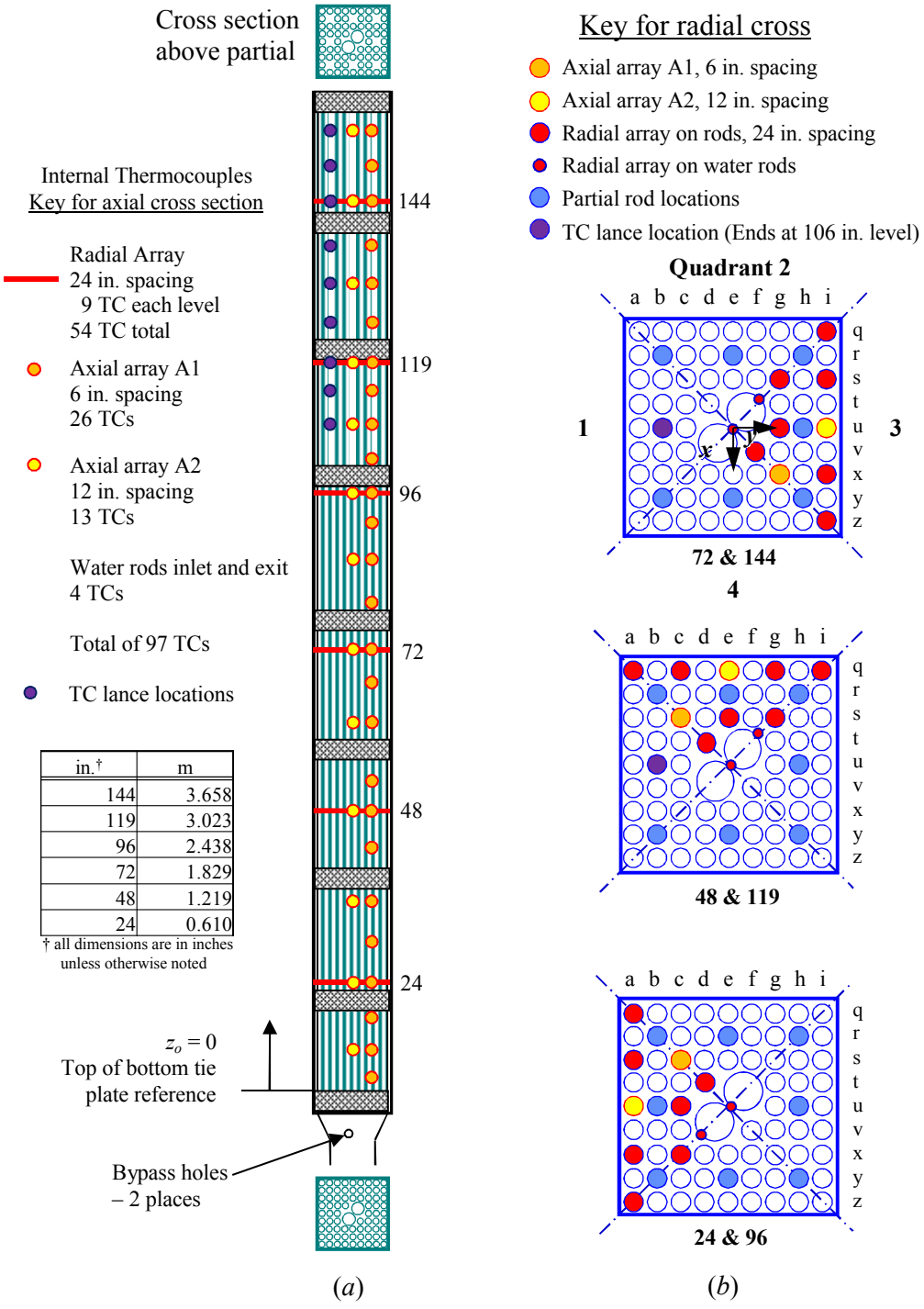

Figure 2.6. Experimental BWR assembly showing as-built *a*) axial and *b*) lateral thermocouple locations.

Based on the need to optimally balance the TC routing through the assembly the axial and radial array TCs were distributed among three separate quadrants relying on the assumption of axial symmetry.

Also shown in Figure 2.6 is the location of the TC lance (for more details see Section 2.3.1.7). The quadrant for the lance deployment was chosen to minimize the possibility of damaging any of the previously installed TCs. The TC spacing on the lance match the elevation of the TCs in the upper portion of the A1 and A2 axial arrays and the radial array at 3.023 m (119 in.) and 3.658 m (144 in.) elevations.

Figure 2.7 shows the definition of the reference coordinate system. The reference origin is defined as being in the center of the top of the bottom tie plate. The *x*-axis is positive in the direction of Quadrant 4 and negative in the direction of Quadrant 2. The *y*-axis is positive in the direction of Quadrant 3 and negative in the direction of Quadrant 1.

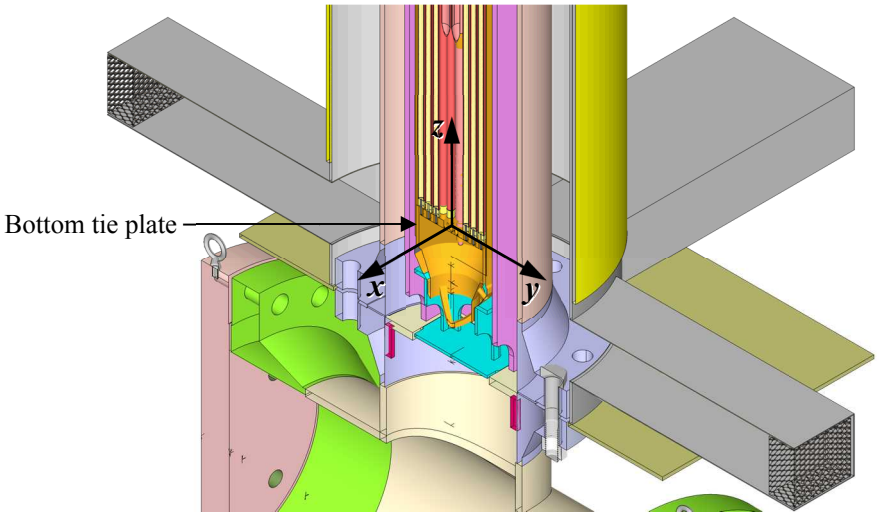

Figure 2.7. Definition of coordinate references in test apparatus.

2.3.1.2 BWR Channel Box TC Locations

The BWR channel box is instrumented with 25 TC's as depicted in Figure 2.8. Twenty-one of the TCs are on the channel faces, 3 are on the corners and one is on the pedestal. The TCs on the faces of the channel box are nominally located at |x|, |y| = 0.069, 0 m (2.704, 0 in.) or |x|, |y| = 0, 0.069 m (0, 2.704 in.) depending on the quadrant in which they are placed. TCs on the corners are located at |x|, |y| = 0.065, 0.065 m (2.564, 2.564 in.). The reference plane, z_o, is measured from the top of the bottom tie plate, the same as the BWR assembly. Multiple TCs on different faces at a given elevation are available to check the axial symmetry assumption at 0.610 m (24 in.) intervals starting at the z = 0.610 m (24 in.) elevation.

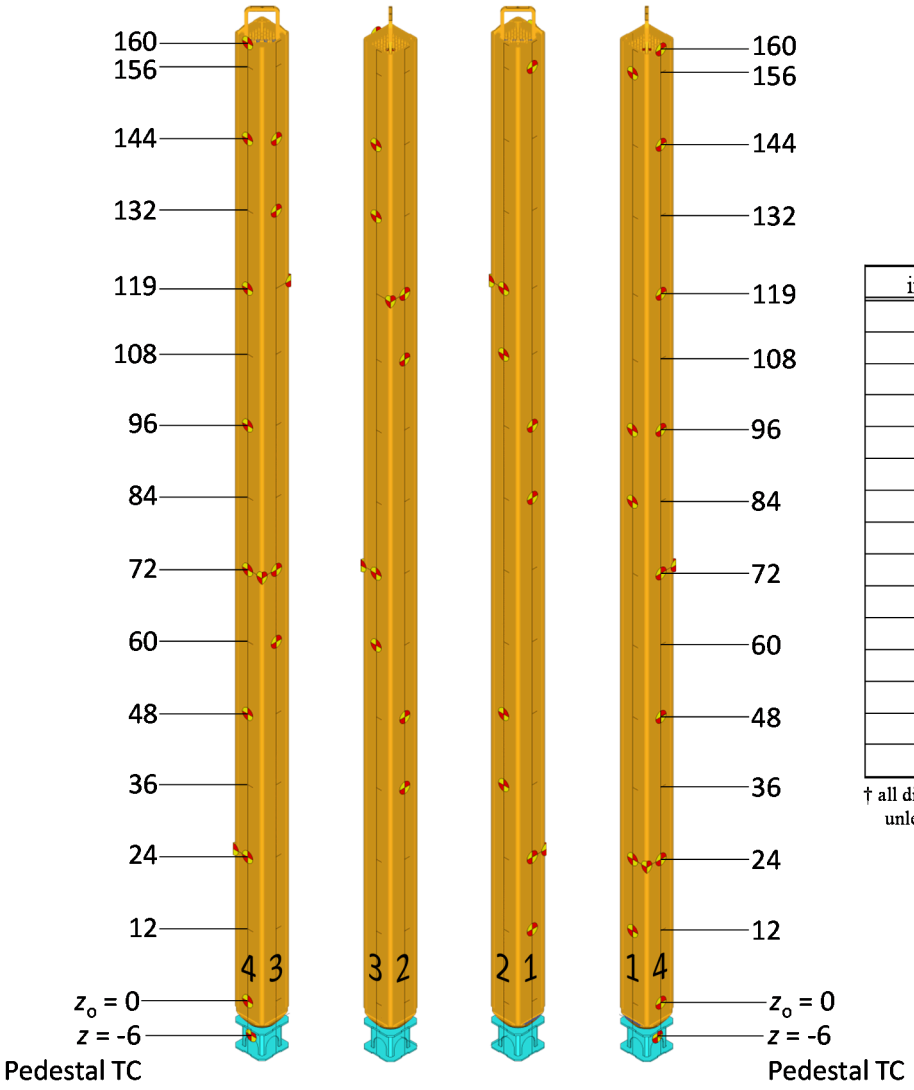

in.†	m
160	4.064
156	3.962
144	3.658
132	3.353
119	3.023
108	2.743
96	2.438
84	2.134
72	1.829
60	1.524
48	1.219
36	0.914
24	0.610
12	0.305
-6	-0.152

† all dimensions are in inches unless otherwise noted

Figure 2.8. BWR channel box showing thermocouple locations.

2.3.1.3 Storage Basket TC Locations

The storage basket is instrumented with 26 TC's as depicted in Figure 2.9. Twenty-two of the TCs are on the basket faces at the same positions as on the channel box, 4 are on the corners (the corner TC at the 4.191 m (165 in.) level does not correspond to a channel box TC) and one is on the basket face at the elevation of the pedestal. TCs located on the basket faces are located at |x|, |y| = 0, 0.089 m (0, 3.5 in.) and |x|, |y| = 0.089, 0 m (3.5, 0 in.). TCs on the corners are located at |x|, |y| = 0.083, 0.083 m (3.281, 3.281 in.). The reference plane, z_o, is measured from the top of the bottom tie plate.

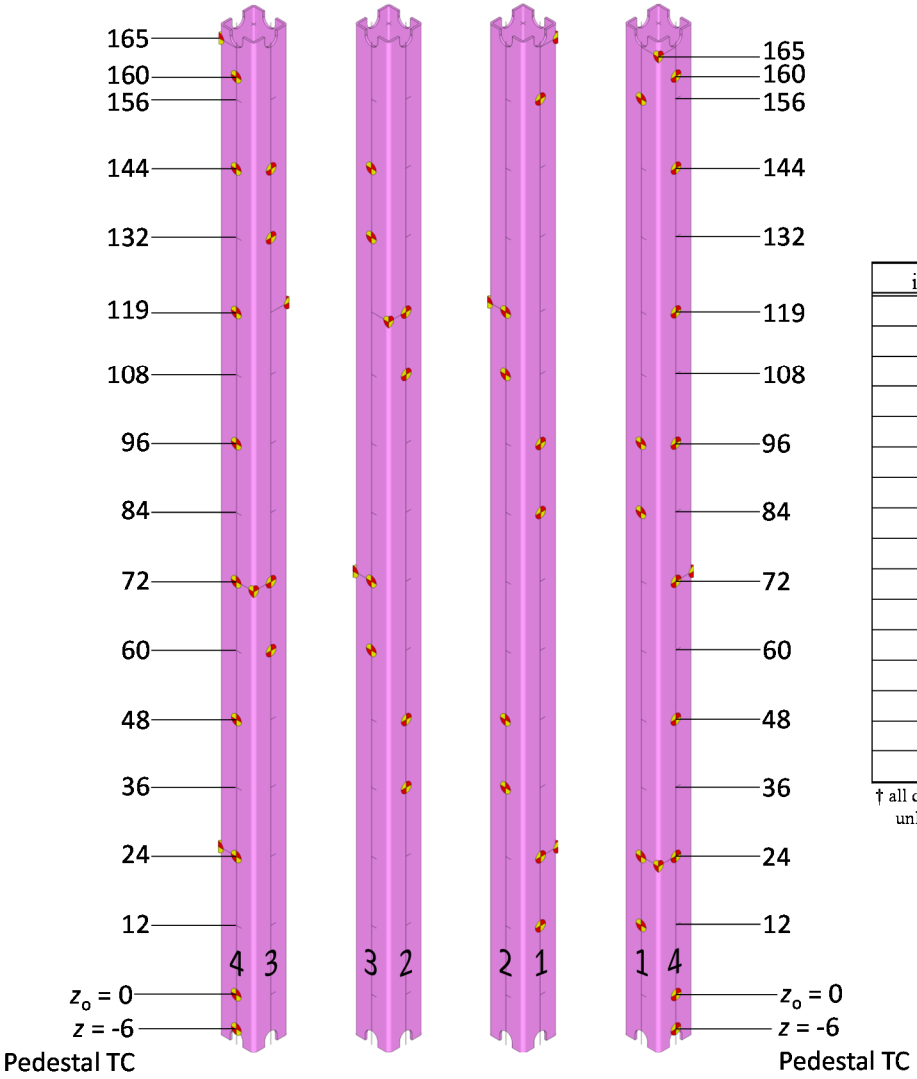

in.†	m
165	4.191
160	4.064
156	3.962
144	3.658
132	3.353
119	3.023
108	2.743
96	2.438
84	2.134
72	1.829
60	1.524
48	1.219
36	0.914
24	0.610
12	0.305
-6	-0.152

† all dimensions are in inches unless otherwise noted

Figure 2.9. Storage basket showing thermocouple locations.

2.3.1.4 Pressure Vessel TC Locations

The pressure vessel is instrumented with 27 TC's as depicted in Figure 2.10. Twenty-four of the TCs are aligned with the TCs on the storage basket faces and 3 are aligned with the TCs on the storage basket corners. TCs aligned with the storage basket faces are located at |x|, |y| = 0, 0.137 m (0, 5.375 in.) and |x|, |y| = 0.137, 0 m (5.375, 0 in.). TCs aligned with the storage basket corners are located at |x|, |y| = 0.097, 0.097 m (3.801, 3.801 in.). The reference plane, z_o, is measured from the top of the bottom tie plate.

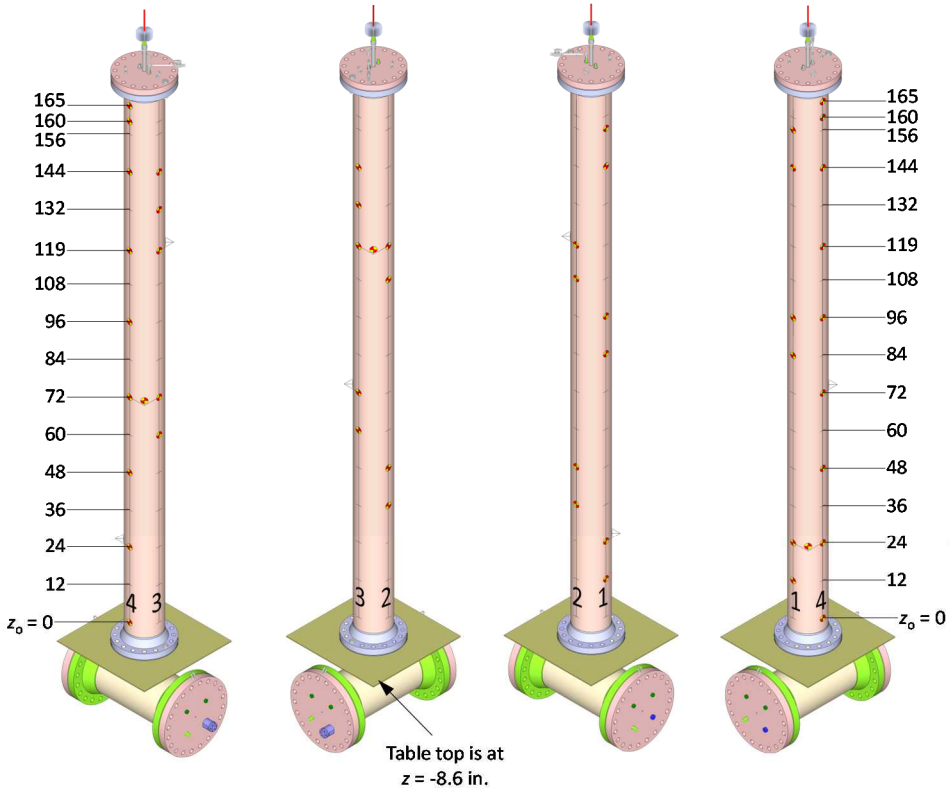

in.†	m
165	4.191
160	4.064
156	3.962
144	3.658
132	3.353
119	3.023
108	2.743
96	2.438
84	2.134
72	1.829
60	1.524
48	1.219
36	0.914
24	0.610
12	0.305

† all dimensions are in inches unless otherwise noted

Figure 2.10. Pressure vessel showing thermocouple locations.

2.3.1.5 Aboveground Configuration Ducting TC Locations

The concentric air flow duct for the aboveground configuration is instrumented with 27 thermocouples depicted in Figure 2.11. Twenty-four of the TCs are aligned with the TCs on the channel box and storage basket faces; 3 are aligned with the corners. The face aligned TCs are located at |x|, |y| = 0, 0.233 m (0, 9.164 in.) and |x|, |y| = 0.233, 0 m (9.164, 0 in.). The corner aligned TCs are located at |x|, |y| = 0.165, 0.165 m (6.480, 6.480 in.). The reference plane, z_o, is measured from the top of the bottom tie plate.

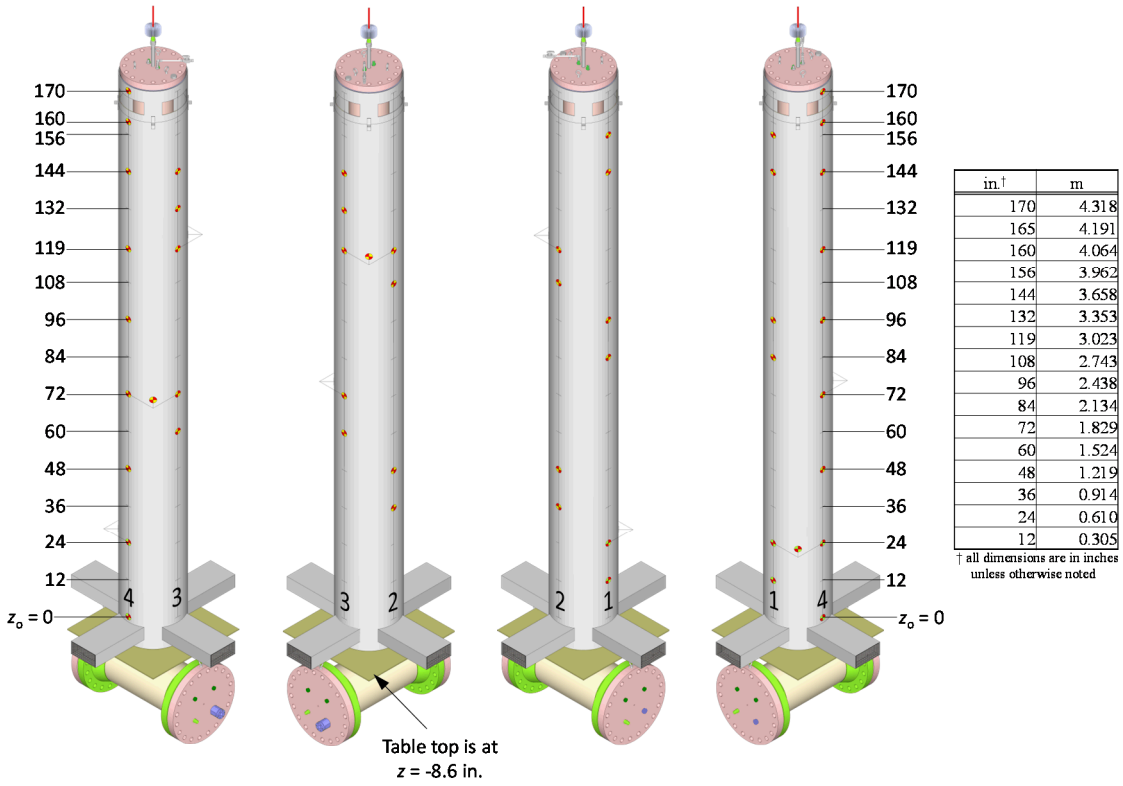

in.†	m
170	4.318
165	4.191
160	4.064
156	3.962
144	3.658
132	3.353
119	3.023
108	2.743
96	2.438
84	2.134
72	1.829
60	1.524
48	1.219
36	0.914
24	0.610
12	0.305

† all dimensions are in inches unless otherwise noted

Figure 2.11. Ducting for aboveground configuration showing thermocouple locations.

2.3.1.6 Gas Temperature TC Locations

Up to 37 TCs are used to measure the temperature of the gas flowing in the various regions of the test apparatus at three different elevations as depicted in Figure 2.12. In anticipation of the next testing phase, the belowground configuration is shown. For the aboveground configuration testing, the outer most gas TCs are installed but the outer shell (shell 2) is not in place. The center region shown in red denotes helium flowing upward while it is heated inside the assembly and storage basket. Moving outward, the region shown in orange depicts helium flowing downward as it cools along the inner pressure vessel wall. A total of 17 TCs are used for gas temperature measurements inside the pressure vessel. More TCs are used at the upper two elevations where higher temperature and temperature gradients are expected.

Moving further outward the region shown in green is air moving upward as it heats along the outer pressure vessel wall. The outer most region, shown in blue, is cool air flowing downward in the belowground configuration. For the aboveground configuration, the outer blue region is open to ambient. The narrow yellow region on the outside of each of the concentric air ducts represents a 6 mm (0.25 in.) thick layer of high temperature insulation.

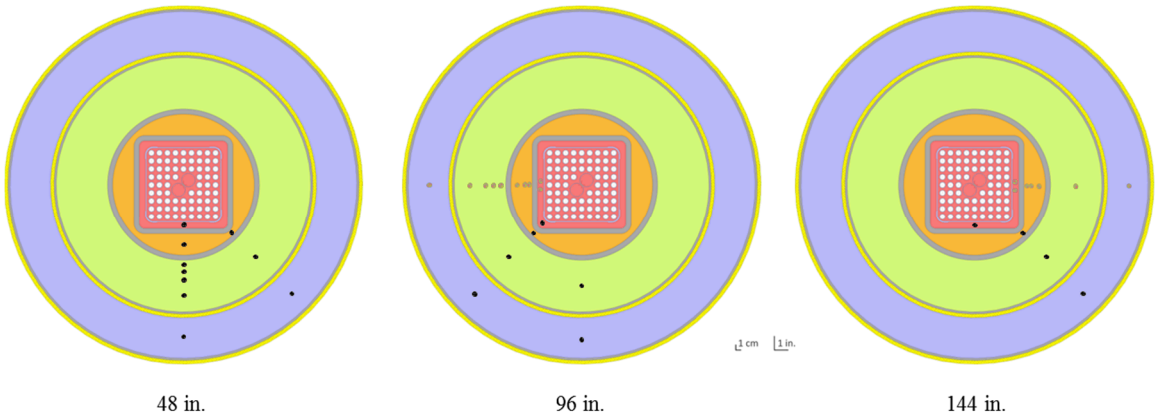

Figure 2.12. Location of thermocouples for gas temperature measurements at elevations of 1.219, 2.438, 3.658 m (48, 96, and 144 in.).

2.3.1.7 TC Lance

A custom TC lance is deployed in the upper portion of the test assembly above a partial length rod as illustrated previously in Figure 2.6. Design details of the lance are shown in Figure 2.13. The design provides for a pressure boundary along the outer surface of the lance with a pressure seal at a penetration in the top flange using standard tube fittings. The lance was made by the same fabricator using the same process and materials as the TC lances that will be used in the full scale High Burnup Dry Storage Cask Research and Development Project [EPRI, 2014]. The TC spacing was designed to correspond with TCs installed on the test assembly heater rod cladding as a means to provide a direct comparison between them. Direct comparisons between TC lance and corresponding clad temperature measurements are expected to aid in the interpretation of the TC lance data generated during the High Burnup Cask Project.

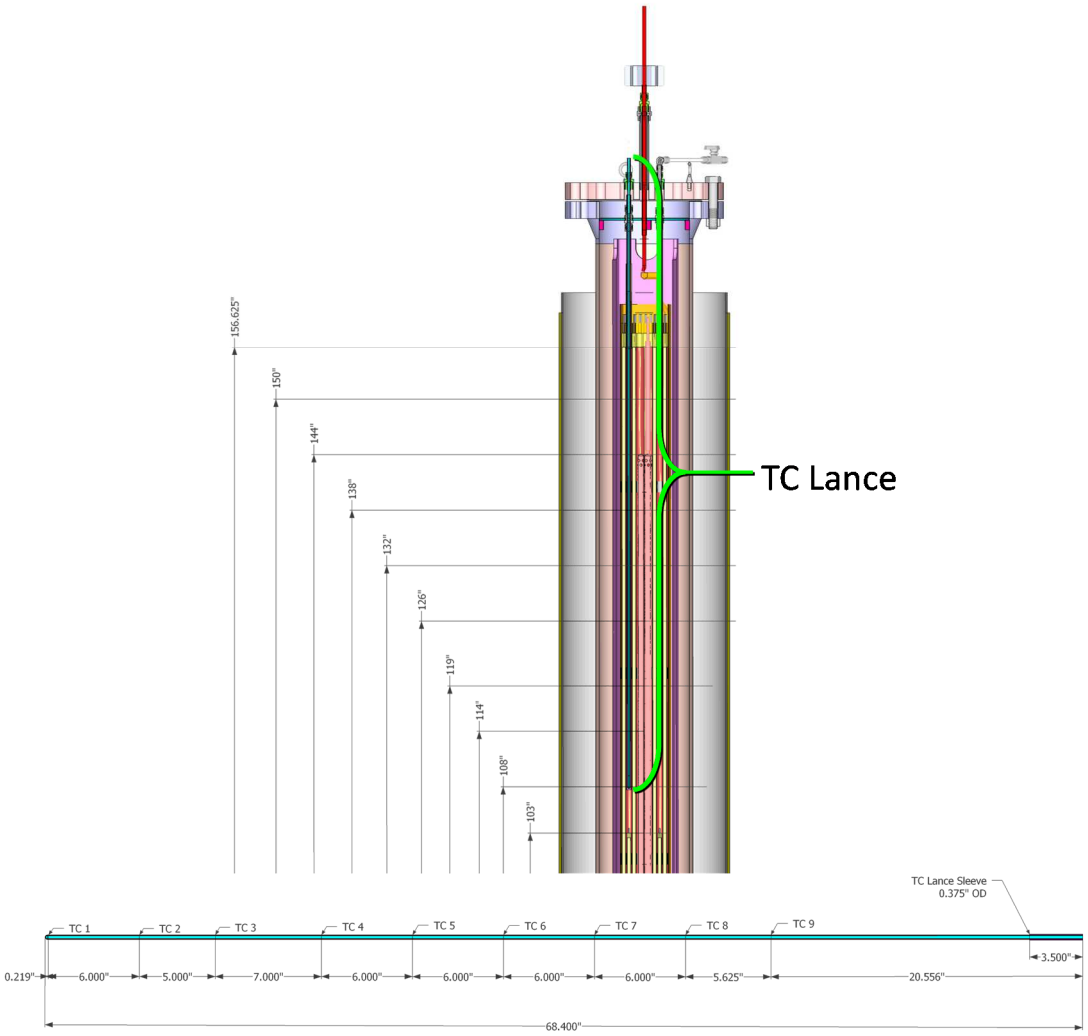

Figure 2.13. TC elevations for the proposed TC lance.

2.3.2 Hotwires

The hotwire anemometers to be used are TSI models 8475 and 8455 where the tip details are shown in Figure 2.14. For scale, the largest shaft diameter shown is 6 mm (0.25 in.). The sensing element of the model 8455 is protected inside of an open cage and is sensitive to flows down to 0.13 m/s (25 ft/min) with a fast response time of 0.2 seconds. The sensing element of the model 8475 is the ball at the tip, which results in sensitivity to flows down to 0.05 m/s (10 ft/min) but with a much larger response time of 5 seconds.

Figure 2.14. Photographs of the two types of hot wire anemometer tips.

2.3.3 Pressure and Pressure Vessel Leak Rates

Two high accuracy 0 to 500 psia absolute pressure transducers (OMEGA PX409-500A5V-XL) were installed in the lower reducing tee. The pressure measurement is made in duplicate due of the importance of the measurement. The experimental uncertainty associated with these gauges is ±0.03% of full scale, or ±0.15 psi.

All penetrations and fittings were selected for the apparatus to have helium leak rates of 1E-6 std. cm^3/s or better at 1 bar. In addition, spiral wound gaskets capable of leak rates of better than 1E-7 std. cm^3/s were used to form the seals at each flange. The ANSI N14.5 leak rate of 1E-4 std. cm^3/s [ANSI, 2014] would result in an observable pressure drop of 4E-3 psi after a one-week period, which is far below the experimental uncertainty of 0.15 psi. Leaks in the as-built apparatus were identified and repaired as best as possible. Ultimately a small helium leak of undetermined origin remained, and a positive pressure control system was implemented to maintain pressure as described next.

2.3.4 Pressure Control

A helium pressure control system was implemented using the high accuracy absolute pressure transducers, three low flow needle valves and three positive shutoff actuator valves under control of the LabView DAC system. Two actuator valves (vent) controlled helium flow out of the vessel, and the third valve (fill) controlled helium flow into the vessel. As the vessel heated up, the expanding helium was vented out the first actuator and needle valve to maintain a constant pressure. A second vent valve (overflow) activated if the vessel continued to pressurize. As steady state was reached, the small helium leak slowly reduced the helium pressure at which point the control system opened the third actuator valve (fill) to allow a small helium flow through the third needle valve. Overall, the pressure control system maintained the pressure constant to ±0.05 psi.

2.3.5 Power Control

A diagram of the test assembly power control system is shown in Figure 2.15 and the details inside the Instrument Panel are shown in Figure 2.16. The electrical voltage and current delivered to the test assembly heaters was controlled to maintain a constant power by a silicon controlled rectifier (SCR). The data acquisition (DAQ) system provided a power setpoint to a PID controller that sent a control signal to the SCR based on the power measurement. The power, voltage and current measurements were collected by the DAQ. The details of the instrumentation used to control and measure the electrical power are provided in Table 2.2.

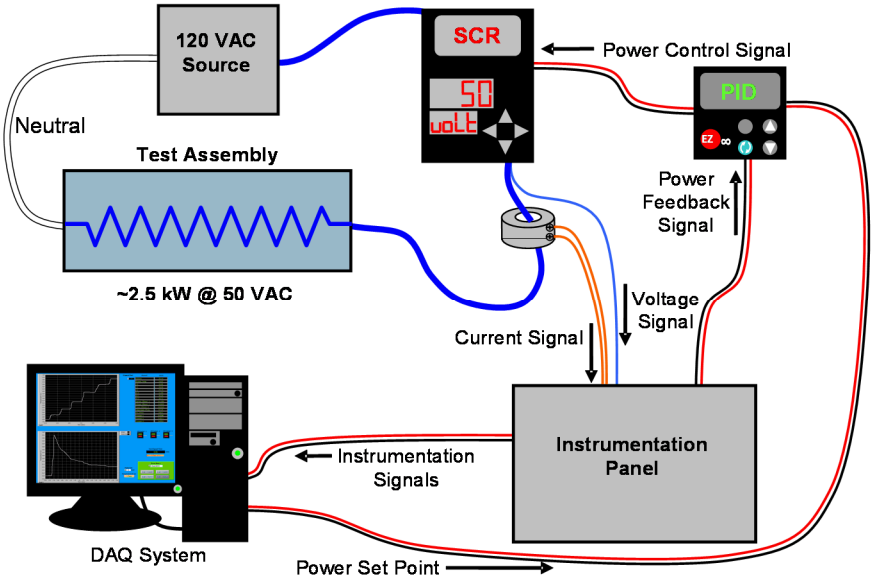

Figure 2.15. Power control system and test circuits.

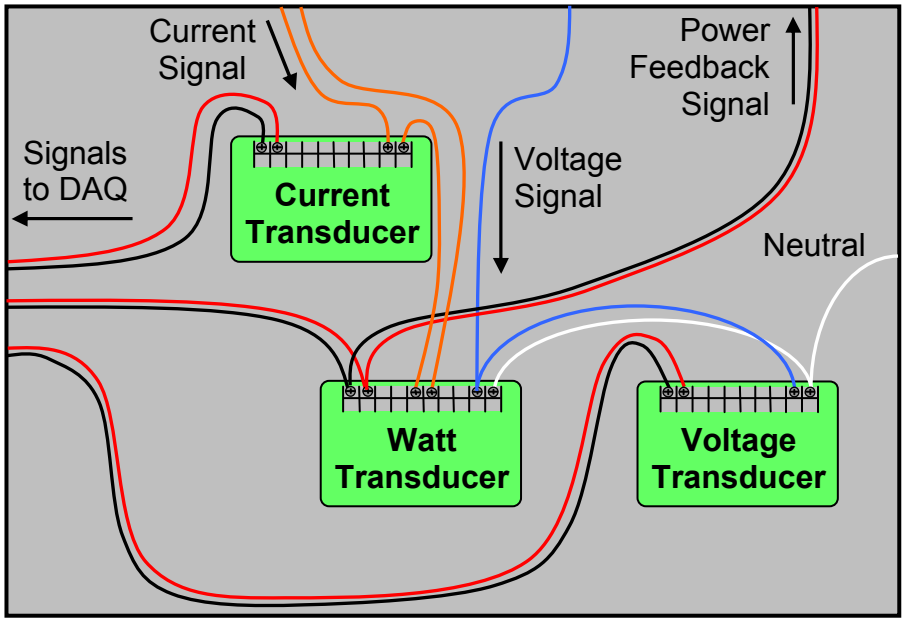

Figure 2.16. Schematic of the instrumentation panel for voltage, current and power measurements.

Table 2.2. List of proposed equipment for power control

Description	Manufacturer	Model
AC Watt Transducer	Ohio Semitronics	PC5-001D
AC Voltage Transducer	Ohio Semitronics	3VTR-001D
AC Current Transducer	Ohio Semitronics	3CTR-010D
PID Controller	Watlow Electric Manufacturing	PM6C1FJ1RAAAAA
SCR Power Controller	Watlow Electric Manufacturing	PC91-F25A-1000

2.4 Air Flow Measurement

The inlet arrangement for the aboveground configuration is shown in Figure 2.17. Four rectangular ducts with as-built cross sectional dimensions of 0.229 m (9.03 in.) by 0.100 m (3.94 in.) conveyed the inlet flow into the simulated cask. Hot wire anemometers were located 0.229 m (9 in.) downstream from the inlet of each duct along the centerline of flow. A single piece of honeycomb was used to straighten the flow at the duct entrance. This plastic honeycomb element had a cell diameter, wall thickness, and flow length of 3.8, 0.1, and 51.6 mm (0.150, 0.004, and 2.030 in.), respectively.

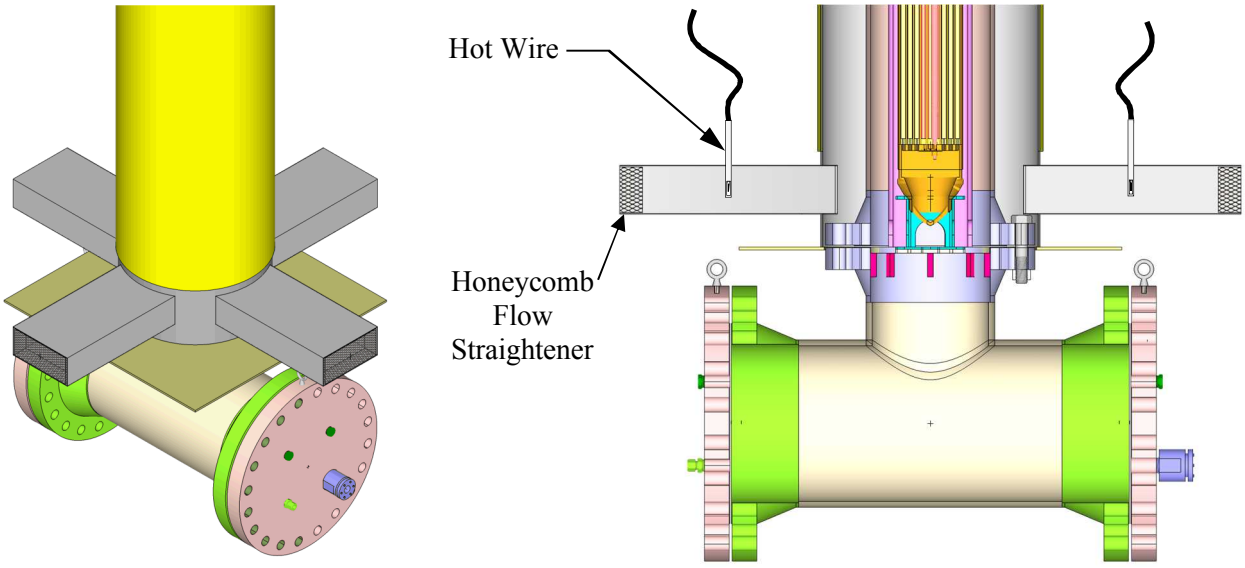

Figure 2.17. Aboveground configuration showing the location of the hot wire anemometer.

2.4.1 Pre-Test Preparation

2.4.1.1 Hotwire Calibrations

Hot wire anemometers were chosen to measure the inlet flow rate because this type of instrument is sensitive and robust while introducing almost no unrecoverable pressure loss. Due to the nature of the hot wire measurement, for best results the probe needs to be placed in the gas flow at the flow inlet before any gas heating has occurred and where there are minimal thermal gradients. A typical placement of the hot wire for the aboveground test configuration is shown in Figure 2.17. One TSI Model 8475 and three TSI Model 8455 hot wire anemometers were used for these tests. A honeycomb element was added to the inlet entrance to reduce the influence of any air flow disturbances within the experimental enclosure on the hot wire measurements.

The hotwire anemometer gas flow velocity probes were calibrated using metered forced flow. A series of unheated calibration runs were performed to calibrate the output of the hot wire anemometer. Detailed traverses in the vertical direction were made in order to provide information on the flow profile. Air flow was metered into each of the inlet ducts individually and the response of the anemometer recorded for a range of flow rates as shown in Figure 2.18. A least-squares regression was used to define the linear coefficients to convert the hot wire anemometer output to a volumetric flow rate during heated testing. The 95% uncertainty to the regression was determined to be ±35 slpm.

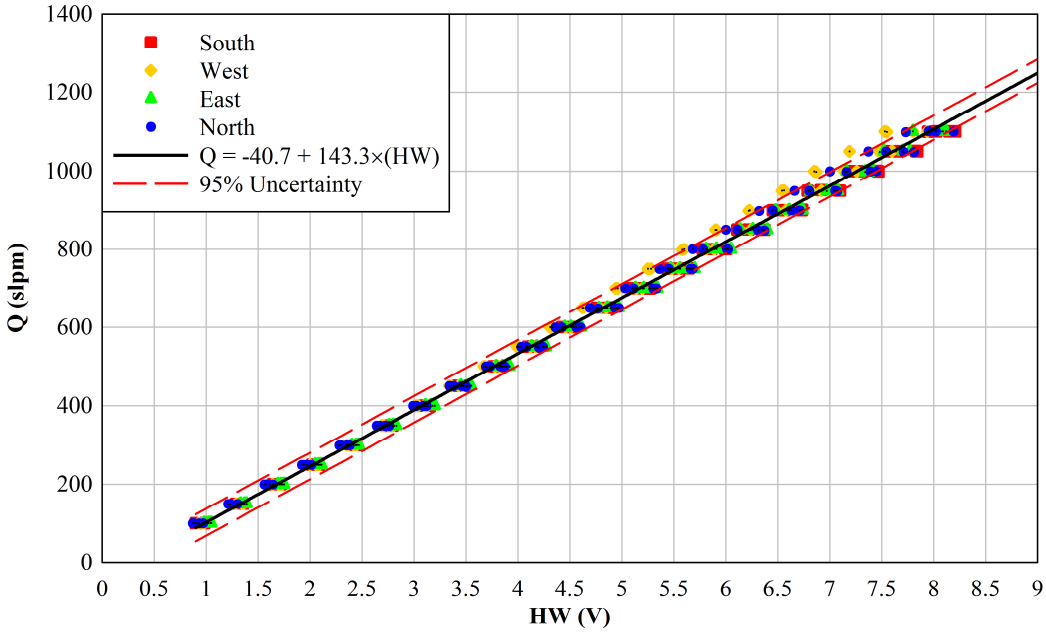

Figure 2.18. Mass flow rate as a function of hot wire output.

2.4.1.2 Pressure Vessel Internal Volume Measurement

The pressure vessel was pressurized with air in a manner that allowed the measurement of the as-built total internal volume. The pressure vessel was first pressurized to 1 bar. The pressure vessel was then slowly pressurized to 2 bar with a high accuracy 0 to 5 liter per minute flow controller (OMEGA FMA 2606A-TOT-HIGH ACCURACY). Two high accuracy 0 to 500 psia absolute pressure transducers (OMEGA PX409-500A5V-XL) were used to monitor the transient fill progression. The transient mass flow and pressure data was used to determine the total internal volume to be 252.0 liters.

3 RESULTS

3.1 Steady State Analyses

A total of fifteen tests were conducted where the apparatus achieved steady state for various assembly powers and helium pressures. The power levels tested were 0.5, 1.0, 2.5, and 5.0 kW. The helium pressures tested were vacuum (0 bar), 1 bar, 4.5 bar and 8 bar absolute. A scaling analysis [Durbin, *et al.*, 2016] showed that elevated powers up to 5 kW were warranted to drive the induced air flow to prototypic levels.

The criterion for steady state was considered met when the first derivative with respect to time of any given TC in the test apparatus was ≤ 0.3 K/h. The steady state values reported here represent the average of data collected between the "start of steady state" and the end of the test.

3.1.1 Peak Cladding Temperature and Air Flow Rate

Figure 3.1 and Figure 3.2 present the steady state data as peak cladding temperature (PCT) and induced air flow rate (per duct), respectively, as a function of power for each helium pressure tested. Figure 3.3 and Figure 3.4 present the same PCT and flow data but as a function of helium pressure for each power tested. Generally, the peak temperatures and induced air flow both increase significantly with power level and decrease slightly with helium pressure. The notable exception is that the peak cladding temperature increased significantly as the helium pressure was decreased from 1 bar absolute to vacuum.

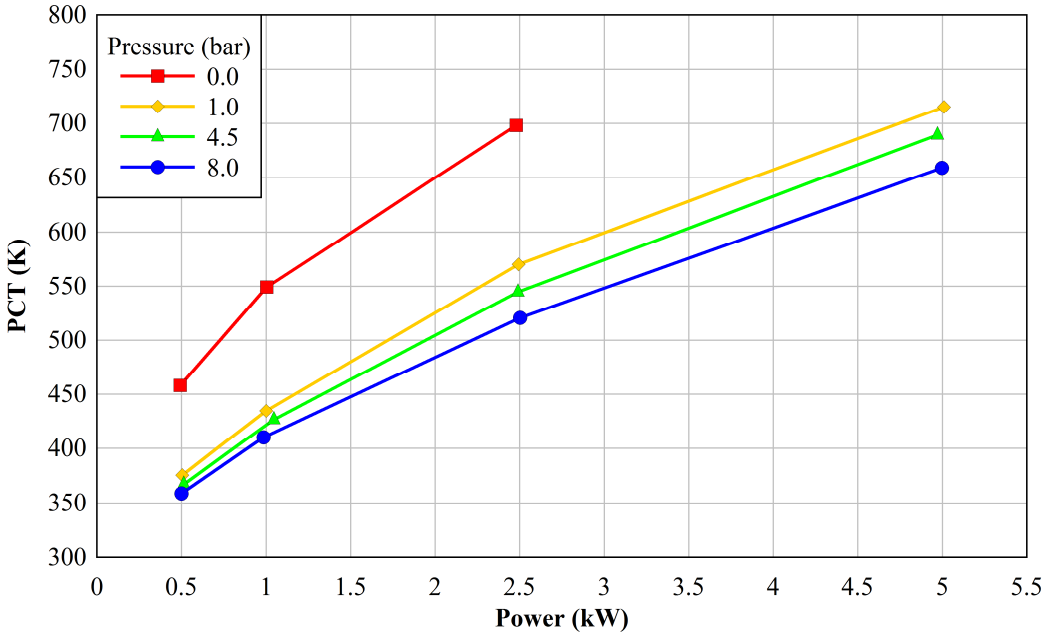

Figure 3.1. Steady state peak cladding temperature as a function of power.

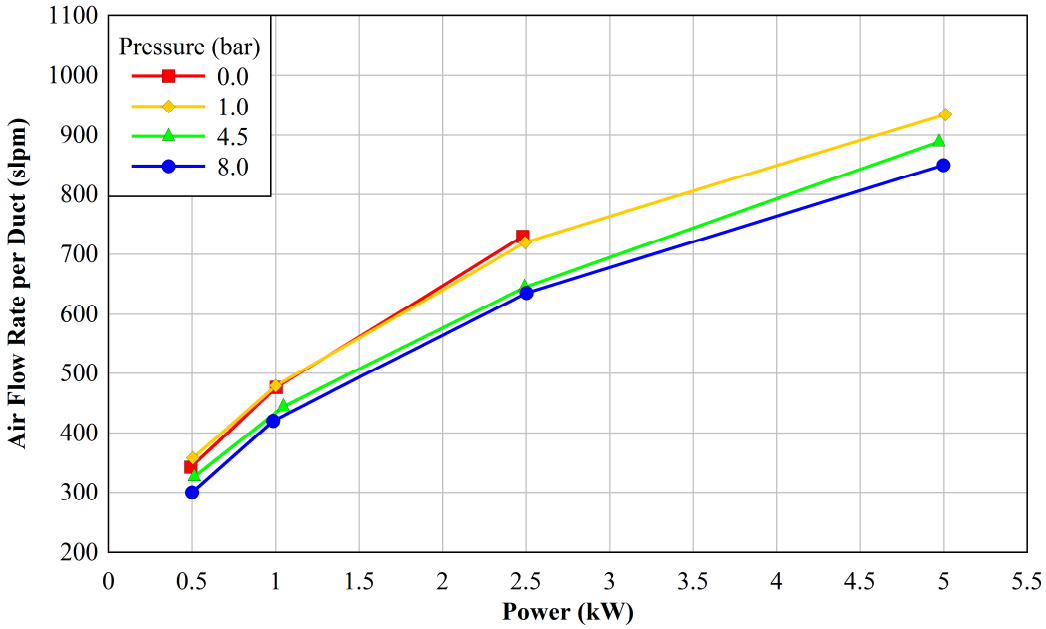

Figure 3.2. Steady state air flow rate per duct as a function of power.

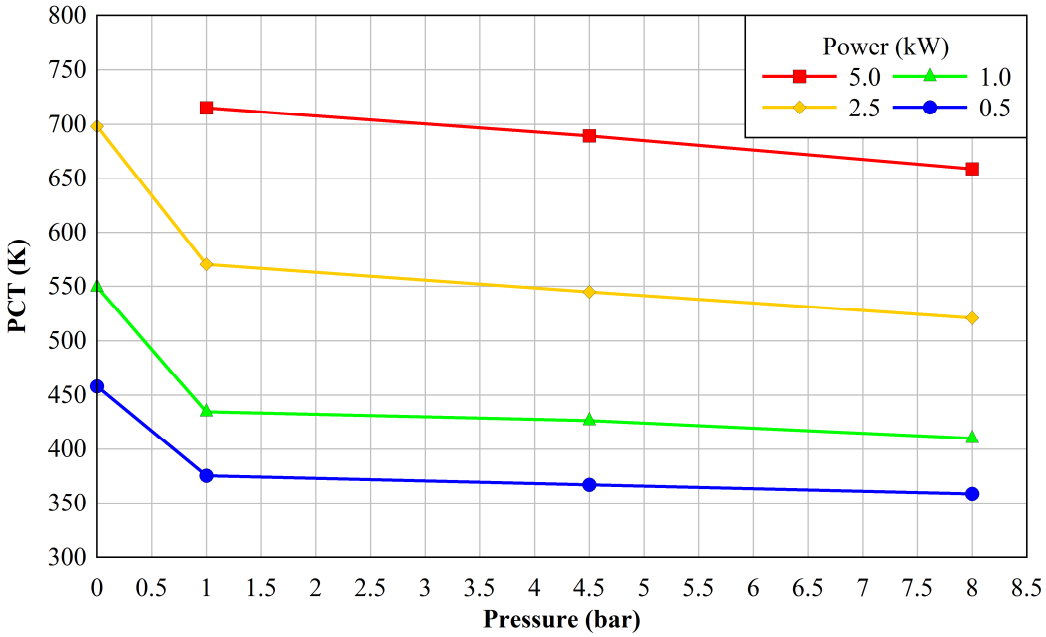

Figure 3.3. Steady state peak cladding temperature as a function of absolute internal helium pressure.

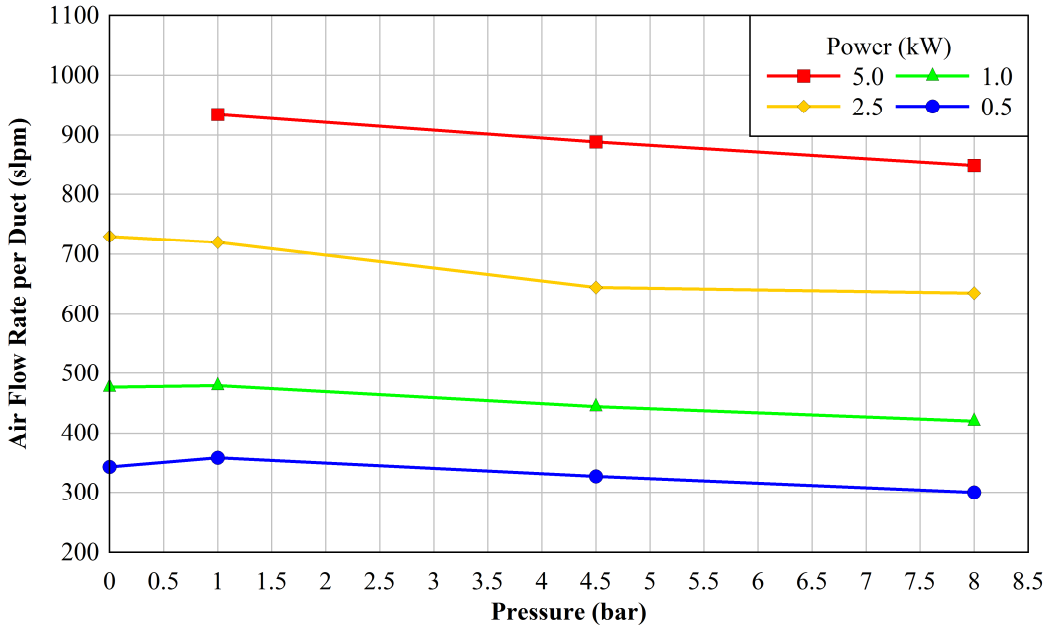

Figure 3.4. Steady state air flow rate per duct as a function of absolute internal helium pressure.

3.1.2 Inlet Duct Flow Profiles

Velocity profiles were collected across the short dimension (0.010 m) at the end of each powered test. The profiles were measured with the hot wire anemometer along the *x*-axis of the duct at 0.229 m (9.00 in.) from the duct entrance as shown in Figure 3.5.

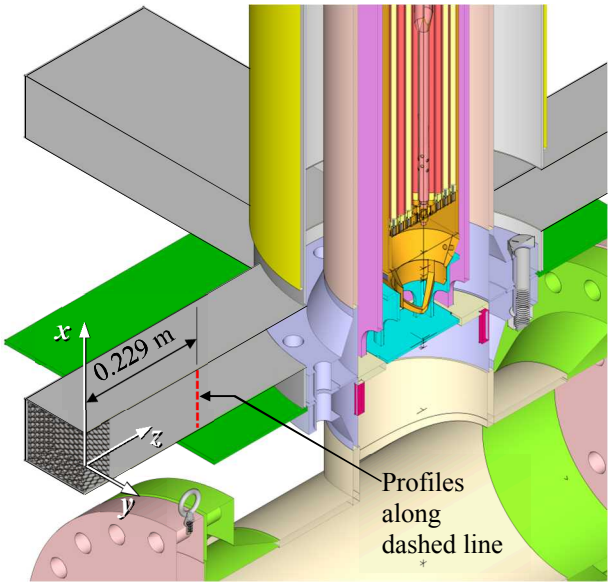

Figure 3.5. Definition of a local coordinate system for inlet duct profiles.

Figure 3.6 shows the steady state mass flow profiles in the South duct derived from the velocity measurements for all power levels and a helium pressure of 8 bar. The average mass flow rate in the duct was calculated by integration across the profile and from the indicated mass flow rate

from earlier, forced flow calibrations. These two measurements of average mass flow rate were within experimental error for all tests.

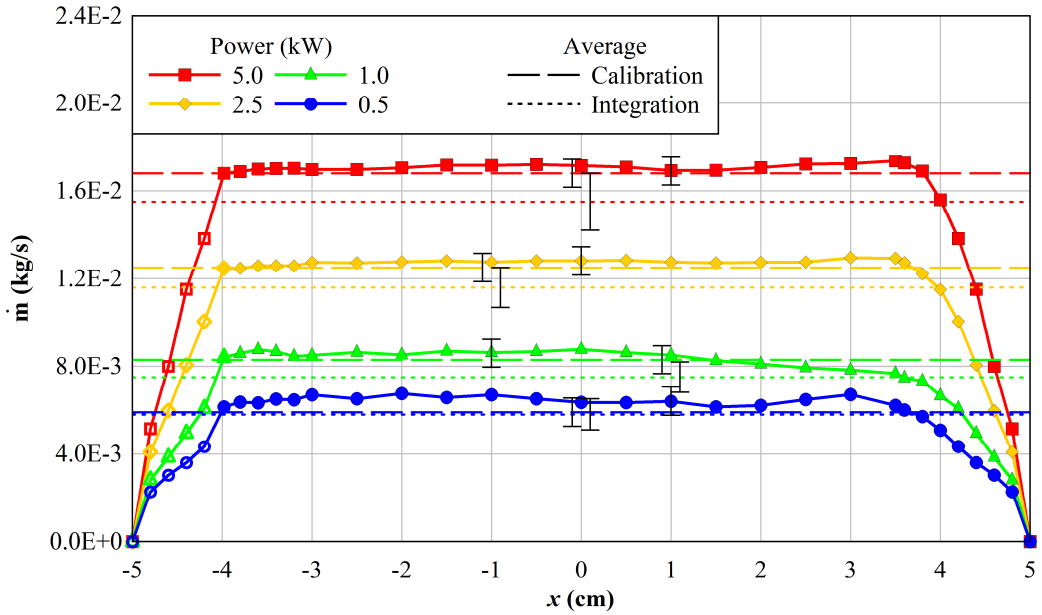

Figure 3.6. Steady state mass flow profiles in the South duct for all power levels and 8 bar helium pressure.

3.1.3 Two-Dimensional Temperature Contours

Figure 3.7 shows 2-D temperature contour plots from the center of the assembly through the basket, pressure vessel, shell 1, and ambient for the high power tests (5 kW) at the three helium pressures tested (1, 4.5, and 8 bar absolute). Figure 3.8 shows 2-D temperature contour plots for the low power tests (0.5 kW) at the four helium pressures tested (0, 1, 4.5 and 8 bar absolute). For both power levels, the peak temperatures decreased with increasing helium pressure. The location of the PCT also shifted from ~1/3 of the assembly height to near the top of the assembly for helium pressures of 0 to 8 bar, respectively.

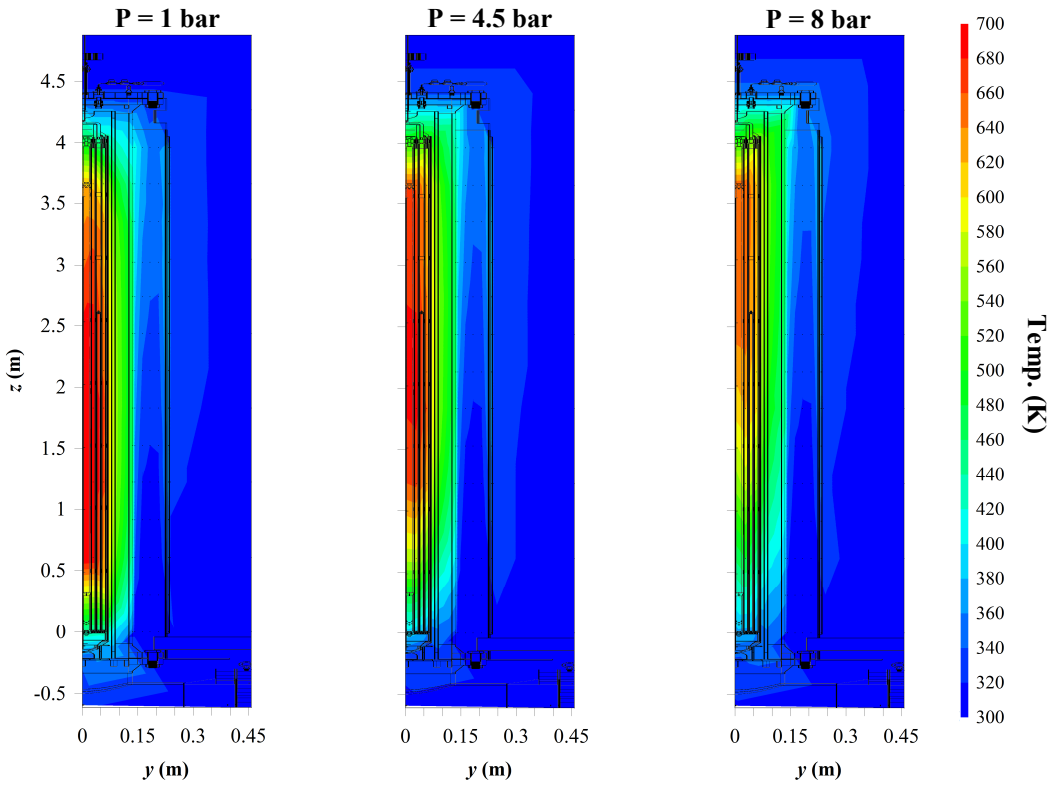

Figure 3.7. Steady state temperature contours for 5 kW at different internal helium pressures.

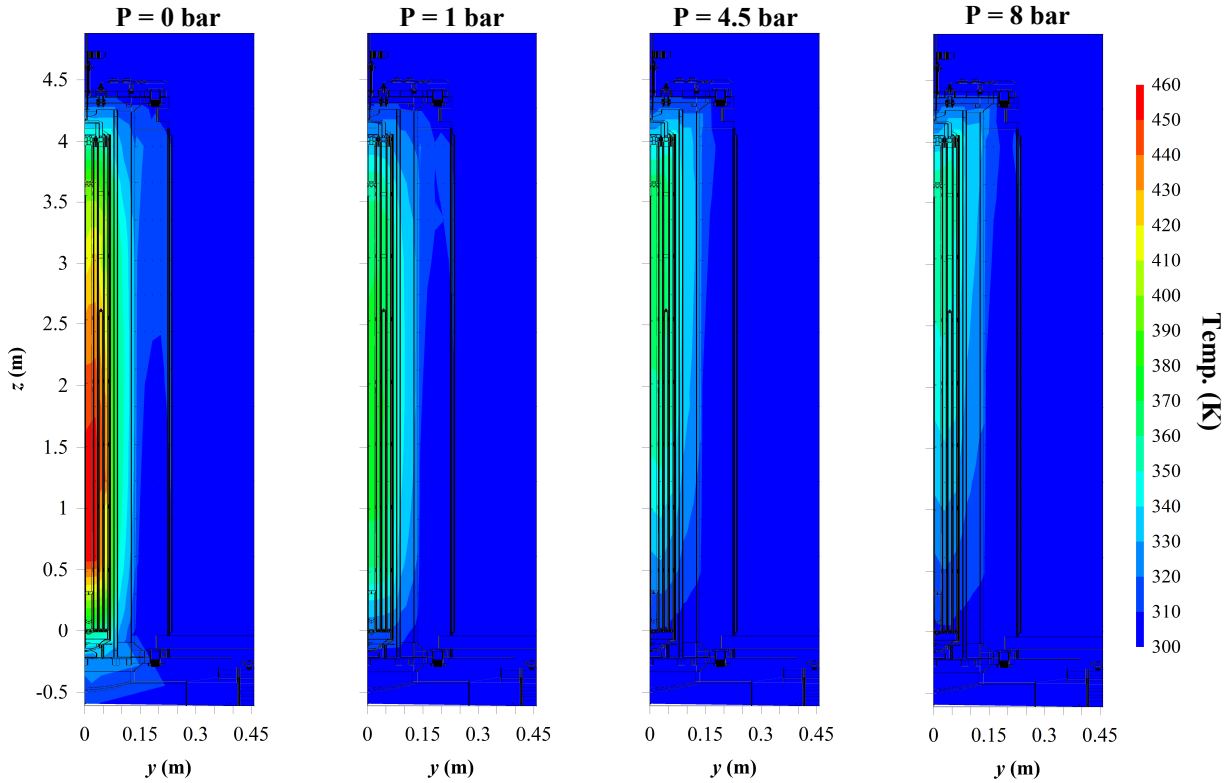

Figure 3.8. Steady state temperature contours for 0.5 kW at different internal helium pressures.

3.1.4 Transverse Temperature Profiles including the TC Lance

Figure 3.9 shows the steady state transverse temperature profile at the z = 3.023 m elevation for the 5 kW and 8 bar case. Figure 3.10 shows a similar steady state transverse temperature profile at the 3.023 m elevation for the 0.5 kW and 8 bar case. The TC lance is located at y = -0.042 m. The assembly TCs for comparison with the TC lance are located starting at x = 0 m and continue along the negative x-direction. Assuming symmetry, the lance is plotted on the x-axis. The TC lance is in good agreement with the interpolated temperature of the two closest assembly TCs.

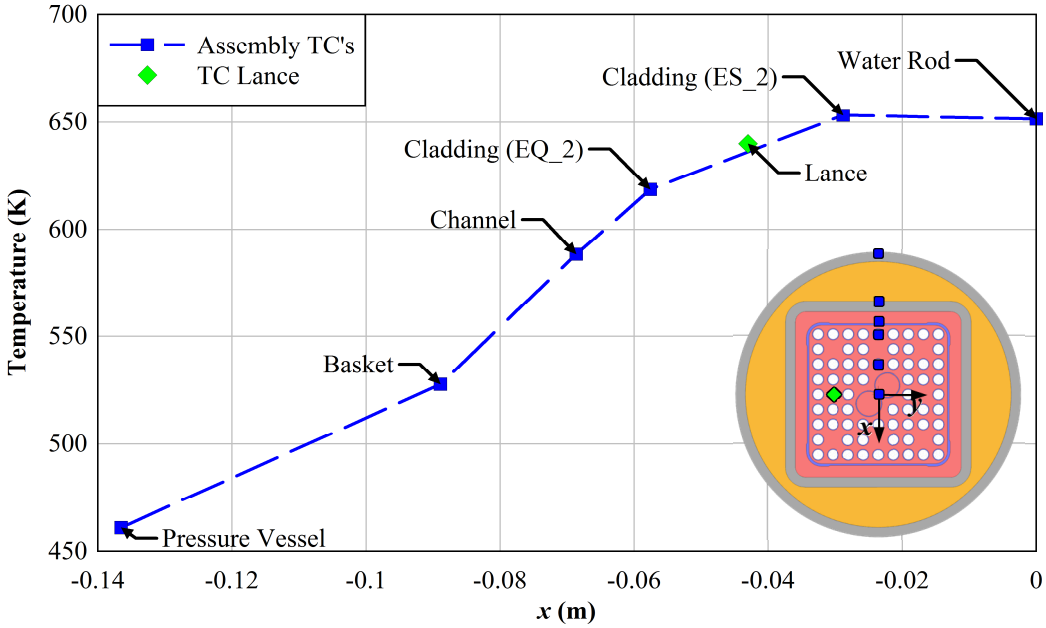

Figure 3.9. Steady state transverse temperature profile at z = 3.023 m (119 in.) for the test conducted at 5 kW and 8 bar.

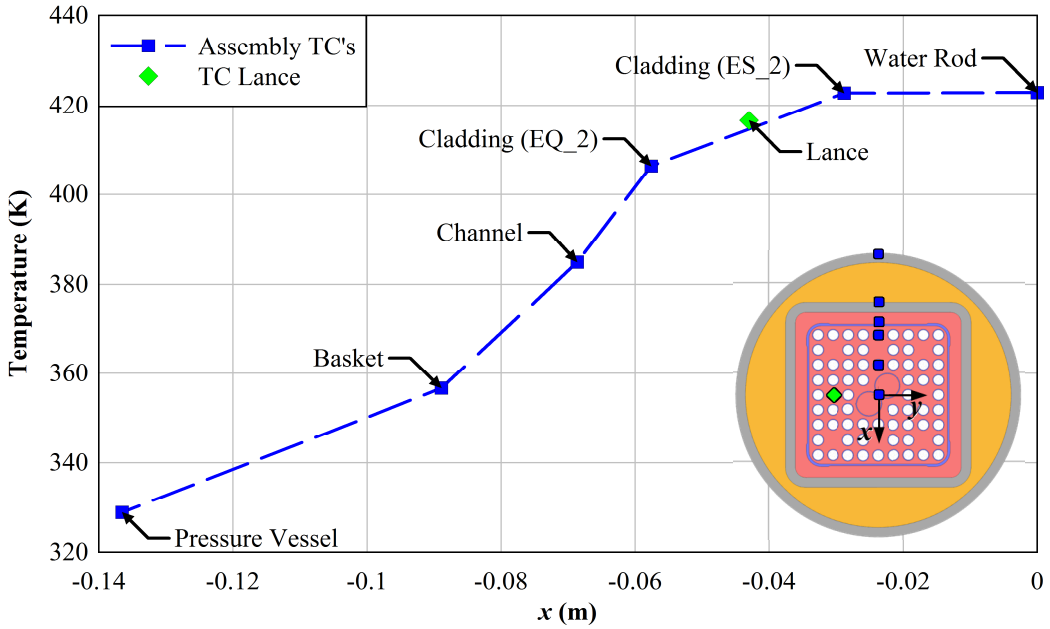

Figure 3.10. Steady state transverse temperature profile at *z* = 3.023 m (119 in.) for the test conducted at 0.5 kW and 0 bar.

3.1.5 Summary Data Tables

The location and value of the peak temperature is presented in the following summary tables for each region of the test apparatus. Tables 3.1 through 3.4 present these peak temperatures and corresponding location along with the measured power, ambient temperature, and induced air flow rate for each power level tested at a given helium pressure.

Table 3.1. Steady state results for the primary assembly measurements at 0 bar

Nominal Power (kW)		Power (kW)	Cladding (K)	Channel (K)	Basket (K)	Vessel (K)	Shell 1 (K)	Ambient (K)	Air Flow Rate (slpm)
0.5	Average	0.492	458	404	361	328	312	299	343
	Max	0.510	459	405	362	330	315	303	390
	Min	0.472	456	403	361	328	311	296	294
	Location		DT_2_48	Channel_4_48	Basket_3_72	PV_2_108	S1_2_119	All	South, East, West
1	Average	1.004	549	470	406	351	323	301	476
	Max	1.041	550	471	407	352	324	303	521
	Min	0.934	549	470	406	351	322	299	425
	Location		DT_1_24	Channel_4_48	Basket_3_72	PV_1_96	S1_2_119	All	South, East, West
2.5	Average	2.479	698	591	493	400	344	297	730
	Max	2.509	699	591	493	400	344	300	777
	Min	2.454	697	590	493	400	344	295	667
	Location		DT_1_24	Channel_4_24	Basket_3_72	PV_1_84	S1_2_119	All	South, East, West

Table 3.2. Steady state results for the primary assembly measurements at 1 bar

Nominal Power (kW)		Power (kW)	Cladding (K)	Channel (K)	Basket (K)	Vessel (K)	Shell 1 (K)	Ambient (K)	Air Flow Rate (slpm)
0.5	Average	0.504	376	359	344	328	312	298	358
	Max	0.525	376	359	344	328	312	300	391
	Min	0.482	375	359	344	328	311	296	330
	Location		FV_3_72	Channel_4_72	Basket_4_96	PV_2-3_119	S1_2_119	All	South, East, West
1	Average	1.001	434	405	378	350	321	299	479
	Max	1.017	435	405	379	350	321	301	509
	Min	0.985	434	404	378	349	321	298	435
	Location		FV_3_72	Channel_4_72	Basket_3_72	PV_2-3_119	S1_2_119	All	South, East, West
2.5	Average	2.493	570	511	461	403	348	300	720
	Max	2.516	570	511	461	403	348	302	761
	Min	2.471	570	511	460	402	347	298	681
	Location		DT_2_48	Channel_3_60	Basket_3_72	PV_2-3_119	S1_2_119	All	South, East, West
5	Average	5.010	715	630	554	467	387	301	935
	Max	5.039	716	631	555	468	389	305	978
	Min	4.969	714	628	553	466	385	299	887
	Location		DT_2_48	Channel_4_48	Basket_3_72	PV_2-3_119	S1_2_119	All	South, East, West

Table 3.3. Steady state results for the primary assembly measurements at 4.5 bar

Nominal Power (kW)		Power (kW)	Cladding (K)	Channel (K)	Basket (K)	Vessel (K)	Shell 1 (K)	Ambient (K)	Air Flow Rate (slpm)
0.5	Average	0.513	367	353	341	326	311	296	327
	Max	0.529	367	353	341	327	312	299	361
	Min	0.489	367	352	340	326	310	293	280
	Location		FV_3_144	Channel_2_119	Basket_3_132	PV_2-3_119	S1_4_159	All	South, East, West
1	Average	1.047	426	399	377	351	323	299	444
	Max	1.073	427	399	377	351	324	302	493
	Min	1.018	425	397	376	350	322	295	382
	Location		FV_3_144	Channel_2_119	Basket_3_132	PV_3_144	S1_4_159	All	South, East, West
2.5	Average	2.491	545	494	451	401	346	300	645
	Max	2.551	546	495	452	402	348	303	686
	Min	2.456	543	492	449	399	345	299	613
	Location		DT_1_96	Channel_2_119	Basket_2_108	PV_2-3_119	S1_3_132	All	South, East, West
5	Average	4.972	689	612	547	465	384	299	888
	Max	5.030	690	613	548	466	386	302	932
	Min	4.910	689	611	547	464	383	297	835
	Location		DT_1_96	Channel_1_84	Basket_2_108	PV_2-3_119	S1_2_119	All	South, East, West

Table 3.4. Steady state results for the primary assembly measurements at 8 bar

Nominal Power (kW)		Power (kW)	Cladding (K)	Channel (K)	Basket (K)	Vessel (K)	Shell 1 (K)	Ambient (K)	Air Flow Rate (slpm)
0.5	Average	0.499	359	347	338	329	312	298	300
	Max	0.516	359	347	338	329	312	299	329
	Min	0.484	358	347	338	329	312	296	259
	Location		FV_3_144	Channel_3_144	Basket_4_159	PV_1_156	S1_4_159	All	South, East, West
1	Average	0.985	410	388	374	356	323	297	420
	Max	1.058	410	389	374	356	324	300	471
	Min	0.967	410	388	373	355	323	294	368
	Location		FV_3_144	Channel_3_144	Basket_4_159	PV_4_159	S1_4_159	All	South, East, West
2.5	Average	2.503	521	477	444	408	349	298	635
	Max	2.547	521	477	444	409	350	303	668
	Min	2.444	521	477	443	408	349	296	596
	Location		FV_3_144	Channel_3_144	Basket_4_159	PV_4_159	S1_4_159	All	South, East, West
5	Average	4.997	659	590	533	466	387	300	849
	Max	5.021	659	590	533	467	387	303	894
	Min	4.956	658	589	532	466	387	299	812
	Location		FV_3_144	Channel_3_144	Basket_3_144	PV_4_159	S1_4_159	All	South, East, West

3.2 Transient Analyses

Figure 3.11 and Figure 3.12 show the peak cladding temperature and average air flow rate per duct for each power tested at 8 bar absolute helium pressure. The air flow rate data is smoothed over a four minute moving window. 95% uncertainties are also presented for select data points, 1% of reading for temperature (±7 K maximum) and ±35 slpm for flow rate.

Steady state conditions were reached in about 15 hours. Figure 3.13 shows the time required to reach steady state as function of power for the various test pressures. The time to steady state was independent of power and helium pressure for the 4.5 bar and 8 bar cases. For the 1 bar helium pressure tests there was a slight dependence on power with 13 hours required at 5 kW and 18 hours required at 0.5 kW. The vacuum tests were the most sensitive to power with up to 31 hours required to reach steady state in the 0.5 kW case.

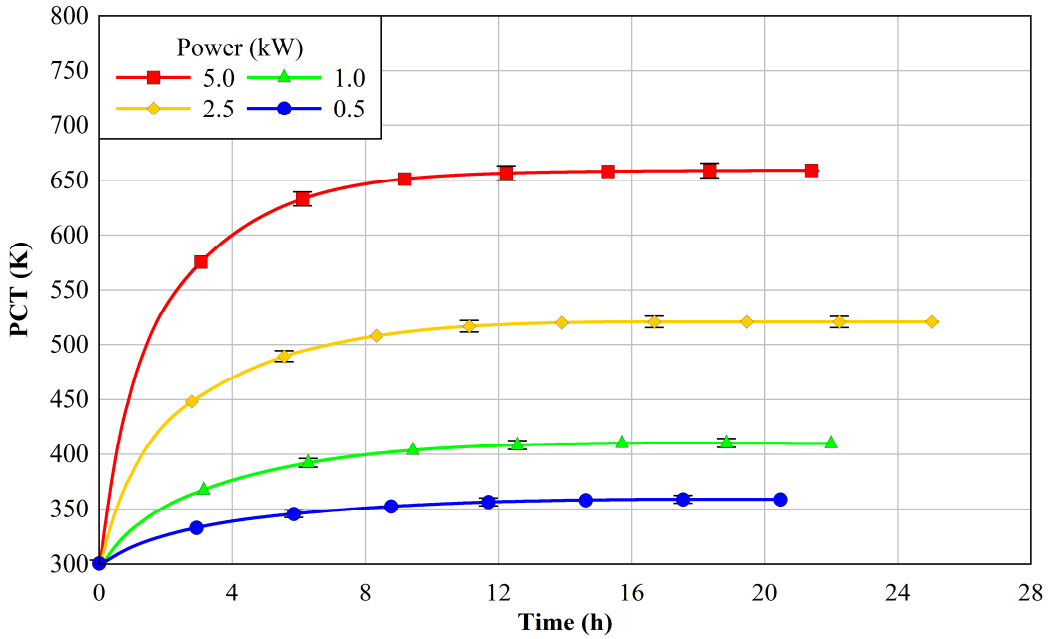

Figure 3.11. Peak cladding temperature as a function of time for tests conducted at 8 bar.

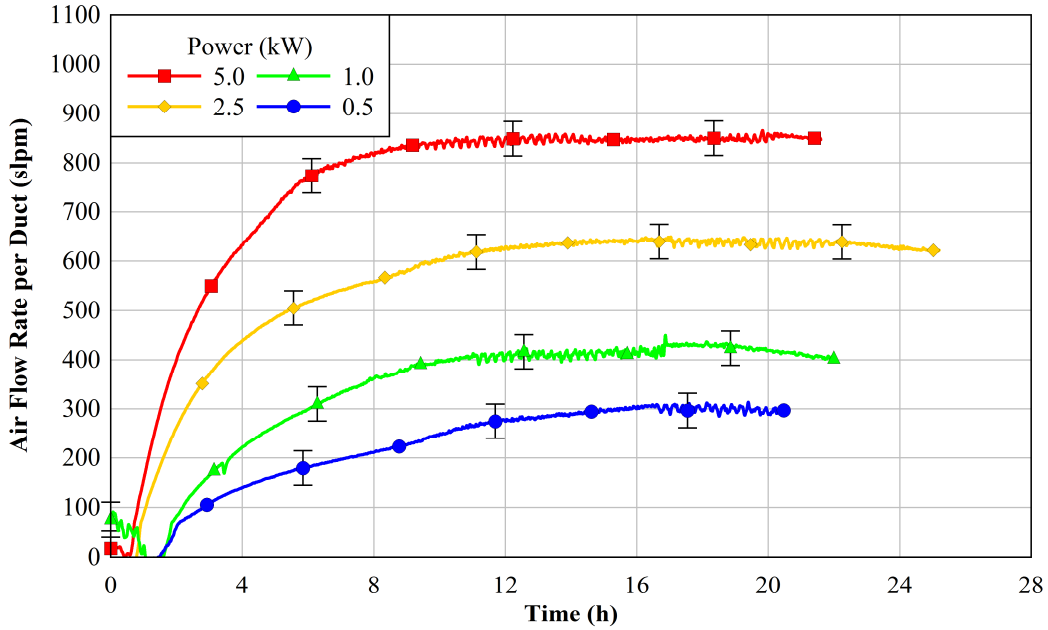

Figure 3.12. Average air flow rate per inlet duct as a function of time for tests conducted at 8 bar.

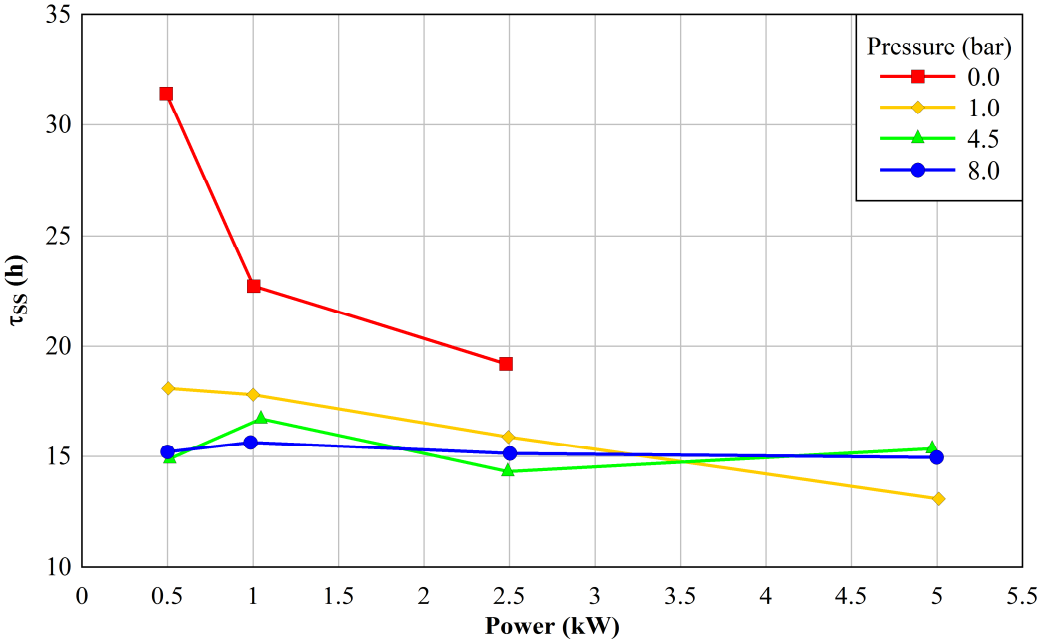

Figure 3.13. Time to reach steady state as a function of power for the various helium pressures tested.

3.2.1 Transient Response of TC Lance and Corresponding Cladding

Figure 3.14 shows the temperature of the TC lance and adjacent cladding TCs (assuming symmetry) as a function of time at the 3.023 m elevation for the 5 kW and 8 bar case. Figure 3.15 shows the temperature of the TC lance and adjacent cladding TCs at the same elevation for the 0.5 kW and 0 bar case. The transient response of the TC lance and the adjacent cladding TCs are similar. The temperature indicated by the lance TC is roughly midway between the adjacent clad TCs. The good agreement provides validation that the TC lance provides an accurate indication of nearby cladding temperatures.

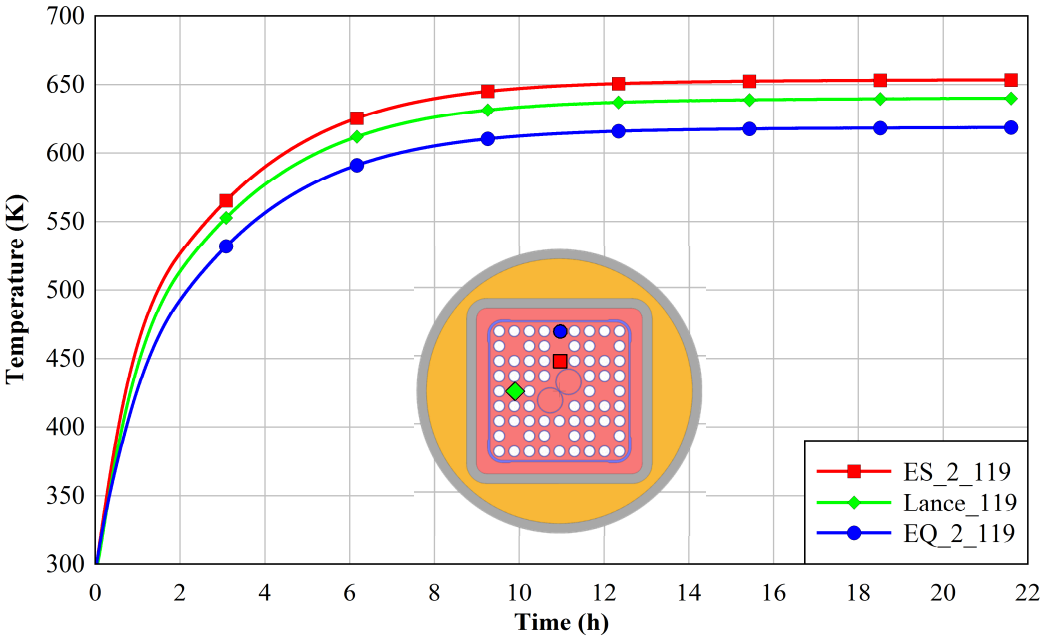

Figure 3.14. Comparison of TC lance and cladding temperatures at *z* = 3.023 m (119 in.) as a function of time for the test conducted at 5 kW and 8 bar.

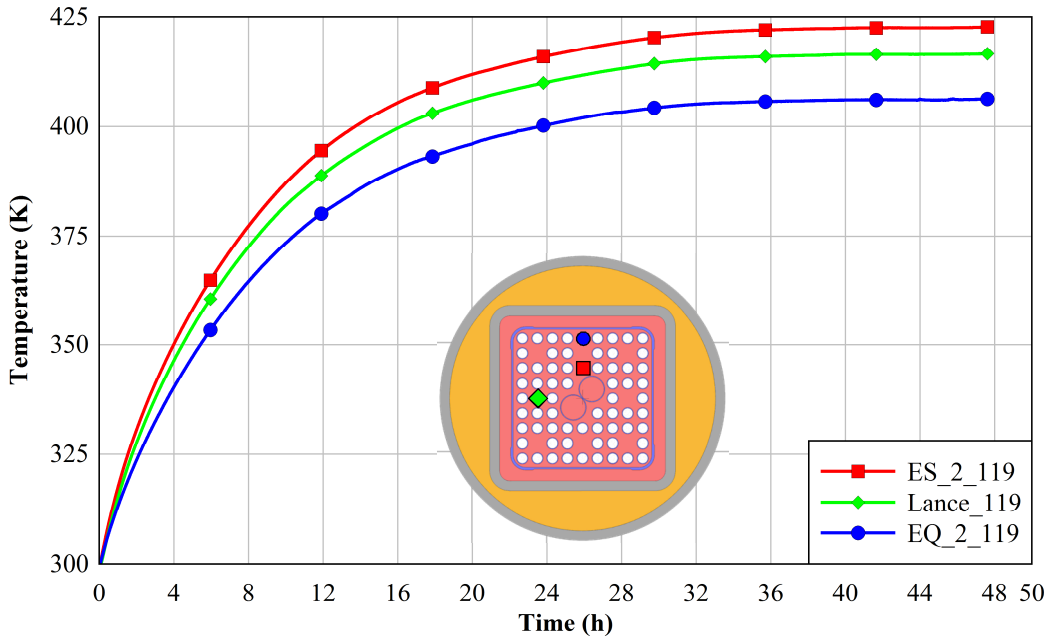

Figure 3.15. Comparison of TC lance and cladding temperatures at *z* = 3.023 m (119 in.) as a function of time for the test conducted at 0.5 kW and 0 bar.

4 SUMMARY

The purpose of this investigation was to produce data sets that can be used to test the validity of the assumptions associated with the calculations used to determine steady-state cladding temperatures in modern dry casks that utilize elevated helium pressure in the sealed canister in an aboveground configuration. A total of fifteen tests were conducted where the apparatus achieved steady state for various assembly powers and helium pressures. The power levels tested were 0.5, 1.0, 2.5, and 5.0 kW. The helium pressures tested were vacuum (0 bar), 1, 4.5, and 8 bar absolute. A previous scaling analysis showed that elevated powers up to 5 kW were warranted to drive the induced air flow to prototypic levels.

An existing electrically heated but otherwise prototypic BWR Incoloy-clad test assembly is deployed inside of a representative storage basket and cylindrical pressure vessel that represents the canister. The symmetric single assembly geometry with well-controlled boundary conditions simplifies interpretation of results. The arrangement of ducting was used to mimic conditions for an aboveground storage configuration in a vertical, dry cask systems with canisters. Radial and axial temperature profiles were measured for a wide range of decay power and helium cask pressures. Of particular interest is the evaluation of the effect of increased helium pressure on heat load.

All steady state peak temperatures and induced flow rates increased with increasing assembly power. Peak cladding temperatures decreased with increasing internal helium pressure for a given assembly power, indicating increased internal convection. In addition, the location of the PCT moved from near the top of the assembly to ~1/3 the height of the assembly for the highest (8 bar absolute) to the lowest (0 bar absolute) pressure studied, respectively. This shift in PCT location is consistent with the varying contribution of convective heat transfer proportional with of internal helium pressure. The highest steady state PCT achieved was 715 K for 5.0 kW and 1 bar helium pressure. This temperature is in the range of the NRC limits for allowable PCT of 673 K for normal operation and 723 K for off-normal operation.

5 REFERENCES

ANSI, American National Standards Institute, "American National Standard for Radioactive Materials – Leakage Tests on Packages for Shipment," ANSI N14.5-2014, June 2014.

Bates, J.M., "Single PWR Spent Fuel Assembly Heat Transfer Data for Computer Code Evaluations," Pacific Northwest Laboratory, Richland, Washington, PNL-5571, January 1986.

Creer, J.M., T.E. Michener, M.A. McKinnon, J.E. Tanner, E.R. Gilbert, R.L. Goodman, "The TN-24P PWR Spent Fuel Storage Cask: Testing and Analyses," EPRI NP-5128 proj. 2406-4, PNL-6054, Pacific Northwest Laboratory, Richland, Washington, April 1987.

Durbin, S.G., E.R. Lindgren, A. Zigh, and J. Solis, "Description of Dry Cask Simulator for Measuring Internal and External Thermal-Hydraulic Performance", SAND2016-0176C, Sandia National Laboratories, Albuquerque, New Mexico, January 2016.

Dziadosz, D., E.V. Moore, J.M. Creer, R.A. McCann, M.A. McKinnon, J.E. Tanner, E.R. Gilbert, R.L. Goodman, D.H. Schoonen, M Jensen, and C. Mullen, "The Castor-V/21 PWR Spent-Fuel Storage Cask: Testing and Analyses," Electrical Power Research Institute, EPRI NP-4887, Project 2406-4, PNL-5917, Pacific Northwest Laboratory, Richland, Washington, November 1986.

EPRI, Electric Power Research Institute, "High Burnup Dry Storage Cask Research and Development Project: Final Test Plan," Contract No.: DE-NE-0000593, February 2014.

Irino, M., M. Oohashi, T. Irie, and T. Nishikawa, "Study on surface temperatures of fuel pins in spent fuel dry shipping/storage casks," IAEA-SM-286/139P, in proceedings of Packaging and Transportation of Radioactive Materials (PATRAM '86), Volume 2, p. 585, International Atomic Energy Agency Vienna, 1987.

Lindgren, E.R. and S.D. Durbin, "Characterization of Thermal-Hydraulic and Ignition Phenomena in Prototypic, Full-Length Boiling Water Reactor Spent Fuel Pool Assemblies after a Complete Loss-of-Coolant Accident", SAND2007-2270, Sandia National Laboratories, Albuquerque, New Mexico, April 2007.

McKinnon, M.A., J.W. Doman, J.E. Tanner, R.J. Guenther, J.M. Creer and C.E. King, "BWR Spent Fuel Storage Cask Performance Test, Volume 1, Cask Handling Experience and Decay Heat, Heat Transfer, and Shielding Data," PNL-5777 Vol. 1, Pacific Northwest Laboratory, Richland Washington, February 1986.

McKinnon, M.A., J.M. Creer , C. L. Wheeler , J.E. Tanner, E.R. Gilbert, R.L. Goodman, D.P. Batala, D.A. Dziadosz, E.V. Moore, D.H. Schoonen, M.F. Jensen, and J.H. Browder, "The MC-10 PWR Spent Fuel Storage Cask: Testing and Analysis", EPRI NP-5268, PNL-6139, Pacific Northwest Laboratory, Richland, Washington, July 1987.

McKinnon, M.A., T.E. Michener, M.F. Jensen, G.R. Rodman, "Testing and Analyses of the TN-24P Spent Fuel Dry Storage Cask Loaded with Consolidated Fuel", EPRI NP-6191 proj. 2813-16, PNL-6631, Pacific Northwest Laboratory, Richland, Washington, February 1989.

McKinnon, M.A., Dodge, R.E., Schmitt, R.C., Eslinger, L.E., & Dineen, G. "Performance testing and analyses of the VSC-17 ventilated concrete cask", EPRI-TR-100305, Electric Power Research Institute, Palo Alto, California, May 1992.